Molecular Therapy
Oncolytics
Original Article

Adoptive T cell immunotherapy for medullary thyroid carcinoma targeting GDNF family receptor alpha 4

Vijay G. Bhoj,[1,2] Lucy Li,[1,2] Kalpana Parvathaneni,[1,2] Zheng Zhang,[1,2] Stephen Kacir,[1] Dimitrios Arhontoulis,[1,2] Kenneth Zhou,[1,2] Bevin McGettigan-Croce,[1,2] Selene Nunez-Cruz,[1,2] Gayathri Gulendran,[1,2] Alina C. Boesteanu,[2] Laura Johnson,[2,7] Michael D. Feldman,[1] Enrico Radaelli,[3] Keith Mansfield,[4] MacLean Nasrallah,[1] Rebecca S. Goydel,[5] Haiyong Peng,[5] Christoph Rader,[5] Michael C. Milone,[1,2,6] and Don L. Siegel[1,2,6]

[1]Department of Pathology and Laboratory Medicine, Perelman School of Medicine, University of Pennsylvania, Philadelphia, PA 19104, USA; [2]Center for Cellular Immunotherapies, Perelman School of Medicine, University of Pennsylvania, Philadelphia, PA 19104, USA; [3]Department of Pathobiology, School of Veterinary Medicine, University of Pennsylvania, Philadelphia, PA 19104, USA; [4]Discovery and Investigative Pathology, Novartis Institute for Biomedical Research, Cambridge, MA 02139, USA; [5]Department of Immunology and Microbiology, The Scripps Research Institute, Jupiter, FL 33458, USA

Metastatic medullary thyroid cancer (MTC) is a rare but often aggressive thyroid malignancy with a 5-year survival rate of less than 40% and few effective therapeutic options. Adoptive T cell immunotherapy using chimeric antigen receptor (CAR)-modified T cells (CAR Ts) is showing encouraging results in the treatment of cancer, but development is challenged by the availability of suitable target antigens. We identified glial-derived neurotrophic factor (GDNF) family receptor alpha 4 (GFRα4) as a putative antigen target for CAR-based therapy of MTC. We show that GFRα4 is highly expressed in MTC, in parafollicular cells within the thyroid from which MTC originates, and in normal thymus. We isolated two single-chain variable fragments (scFvs) targeting GFRα4 isoforms a and b by antibody phage display. CARs bearing the CD3ζ and the CD137 costimulatory domains were constructed using these GFRα4-specific scFvs. GFRα4-specific CAR Ts trigger antigen-dependent cytotoxicity and cytokine production *in vitro*, and they are able to eliminate tumors derived from the MTC TT cell line in an immunodeficient mouse xenograft model of MTC. These data demonstrate the feasibility of targeting GFRα4 by CAR T and support this antigen as a promising target for adoptive T cell immunotherapy and other antibody-based therapies for MTC.

INTRODUCTION

Medullary thyroid carcinoma (MTC) is the third most common thyroid malignancy, with both sporadic and hereditary forms.[1,2] Unlike the majority of thyroid cancers that arise from the follicular epithelium of the thyroid, MTC arises from the malignant transformation of parafollicular cells (also known as C cells) within the thyroid, which are neuroendocrine cells that secrete the polypeptide hormone calcitonin.[1,2] The hereditary form of MTC, which comprises approximately 25% of cases, is associated with germline mutations in the *RET* proto-oncogene, and this form can be associated with tumors in the adrenal or parathyroid glands as part of the multiple endocrine neoplasia type 2 (MEN2) syndrome.[1,2] Sporadic cases of MTC, which typically present at a more advanced stage at diagnosis compared with hereditary forms, are also frequently associated with somatic mutations within the *RET* proto-oncogene, supporting the underlying importance of this gene in MTC.[3] While early-stage disease can be cured by total thyroidectomy, therapeutic options are limited for patients with metastatic disease, where the 5-year survival is less than 40%.[2,3] Unlike in other forms of thyroid cancer of follicular origin, there is no role for therapeutic radioactive iodine in MTC. There is also a limited role for cytotoxic chemotherapy in this disease, and a role for immunotherapy is unknown; in general, the prognosis for metastatic MTC remains poor.[4] Recently, several small-molecule tyrosine kinase inhibitors (TKIs) have been introduced for the treatment of metastatic MTC.[5] These agents result in objective responses in only a subset of patients (27%–40%); however, the long-term durability of these responses is unclear.[6,7] Thus, there remains a strong need for new therapies for MTC.

Chimeric antigen receptor (CAR) technology, in which an extracellular antigen-binding domain from an antibody is fused to cytoplasmic signaling domains of the T cell receptor and costimulatory receptors, has shown notable promise for the treatment of advanced B cell malignancies.[8] When expressed on a patient's own T cells, a CD19-specific

Received 28 March 2020; accepted 19 January 2021;
https://doi.org/10.1016/j.omto.2021.01.012.

[6]These authors contributed equally

[7]Present address: GlaxoSmithKline, Brentford, UK

Correspondence: Vijay G. Bhoj, MD, PhD, South Tower Pavilion, 8-111, 3400 Civic Ctr. Blvd., Philadelphia, PA 19104, USA.
E-mail: vbhoj@pennmedicine.upenn.edu
Correspondence: Don L. Siegel, PhD, MD, South Tower Pavilion, 9-112, 3400 Civic Ctr. Blvd., Philadelphia, PA 19104, USA.
E-mail: siegeld@pennmedicine.upenn.edu

CAR directs those T cells to specifically kill CD19 antigen-expressing cancer cells and normal B cells, leading to complete and durable remission of disease even in late-stage cancer patients.[9–11] While highly effective in B cell malignancies, applications of CAR T-based therapies to other malignancies, especially solid tumors, has been hampered by the availability of suitable target antigens with expression that is limited to tumors and to tissues with replaceable functions.[12,13] Early-phase studies with several CARs for the treatment of solid tumors have led to severe adverse events due to target expression on critical normal tissues.[12,14]

Through RNaseq analysis of MTC, we identified the RET-associated receptor of the glial-derived neurotrophic factor (GDNF) receptor (GFR) family, GFRα4, as an MTC-associated antigen with highly restricted expression in humans. There are four known GDNF receptors: GFRα1, GFRα2, GFRα3, and GFRα4.[15] Unlike the other family members, which display widespread expression within the brain and central nervous system of mammals, GFRα4 expression appears restricted to normal parafollicular cells within the thyroid.[16] GFRα4 is predicted to produce 3 isoforms in humans, two GPI-linked membrane-bound forms (a and b), differing by 47 amino acids in the extracellular region, and a putative secreted form, GFRα4c.[16] Mice bearing deletions of GFRα4 appear healthy, with no obvious developmental abnormalities.[17] GFRα4 knockout mice exhibit defects in calcitonin regulation, suggesting that GFRα4 is critical for normal parafollicular cell function; however, the role of calcitonin in normal human physiology is unknown.[18] Although calcitonin infusion can induce some hypocalcemia, patients with extremely low or absent calcitonin secretion following total thyroidectomy or MTC patients with extremely high calcitonin concentrations fail to show any obvious signs of calcium or bone abnormalities.[19]

Based on the expression of GFRα4 by MTC and otherwise restricted expression to normal parafollicular cells, along with the observation that elimination of normal parafollicular cells through thyroidectomy does not lead to adverse clinical effects, we hypothesize that GFRα4 is a useful target antigen for CAR-based T cell immunotherapy for MTC. We therefore developed single-chain variable fragments that permit specific targeting of GFRα4 by CAR T therapy for MTC. In this report, we present the results of preclinical studies that include the feasibility of targeting this receptor via CAR along with an in-depth evaluation of GFRα4 expression in normal human tissues to support further investigation of GFRα4-specific immunotherapy in the treatment of MTC.

RESULTS

Target identification and validation

RNA-seq analysis was performed on a tumor sample from a 49-year-old male with metastatic MTC; the patient's tumor harbored an acquired RET-activating mutation, Glu632-Leu633 deletion, in one allele of *RET*[20] in addition to a germline (Tyr791Phe) variant in the other allele. Gene expression of his tumor compared to publicly available normal tissue expression data generated by GTEx revealed that the gene *GFRA4* was highly expressed in his MTC (Figure 1A) and that this gene is one of the highest differentially expressed genes, relative to normal tissues. Consistent with its expression in MTC, which arises from thyroid parafollicular cells, *GFRα4* RNA expression also showed relative thyroid specificity by RNA *in situ* hybridization and qRT-PCR of normal tissues (Figures 1B–1D; Table S1). Although *GFRα4* RNA was detected in testis by qPCR, this was not observed by *in situ* hybridization. Interestingly, a GFRα4 expression signal is also identified in testis according to the Human Protein Atlas, although the level is far lower than in normal thyroid.[21] Lindahl et al.[16] did not detect *GFRA4* mRNA in human testis by endpoint RT-PCR. Thus, the discrepancy in our results may reflect an artifact of the qPCR assay or a level that is below the level of sensitivity of some assays (i.e., ISH, RT-PCR). Consistent with Lindahl et al.,[16] we found *GFRα4* mRNA expression in 7 out of 7 cases of MTC evaluated (Figure 1C; Figure S1) as well as the MTC-derived TT and MZ-CRC1 cell lines, although the level was 100-fold lower in MZ-CRC1. As expected, *GFRα4* expression was seen in scattered cells within normal thyroid parenchyma but not the follicular epithelium. GFRα4 mRNA expression examined by ISH in samples from cynomolgus macaques also showed thyroid specificity and is summarized in Table S2.

RET-driven signaling is thought to play a central role in both hereditary and sporadic forms of MTC. Indeed, TKIs are thought to control MTC growth by inhibiting RET signaling, and RET knockdown in TT cells was shown to inhibit growth in culture.[22,23] Since RET is known to complex with GFR family members at the cell surface, we sought to determine if GFRα4 may be required to maintain stable RET expression, and consequent signaling, in MTC cells. If GFRα4 is required, we reasoned that the risk of tumor escape due to antigen loss following GFRα4-directed immunotherapy would be lower. However, while knockdown of RET inhibited TT cell proliferation as previously published, knockdown of GFRα4 had no effect (Figure S2).

Isolation and validation of GFRα4-specific antibody

As no antibodies were available for GFRα4 that were shown to bind well to both of its cell-surface GPI-linked isoforms, we screened a naive rabbit-human chimeric Fab library to isolate GFRα4-specific binders that could be used to generate scFv for incorporation into a CAR. After 4 rounds of panning against microplate-bound human GFRα4 isoform a or b in the presence of a 10-fold mass excess of soluble GFRα1, GFRα2, and GFRα3 proteins to avoid isolating cross-reactive antibodies, we isolated 2 unique clones, termed P4-6 and P4-10, that each bound to both isoforms of GFRα4 but not to GFRα1, GFRα2, and GFRα3 (Figure S3).

P4-6 and P4-10 Fabs were assessed for cross-reactivity to other human membrane proteins using a membrane proteome array consisting of over 4,500 unique human membrane proteins (performed by Integral Molecular, Philadelphia, PA, USA). P4-10 demonstrated reactivity against only GFRα4, whereas P4-6 showed reactivity against GFRα4 as well as SYT2, a synaptic vesicle membrane protein involved in vesicle exocytosis (Figure S4). Given its specificity, we conducted pre-clinical CAR T cell studies using P4-10.

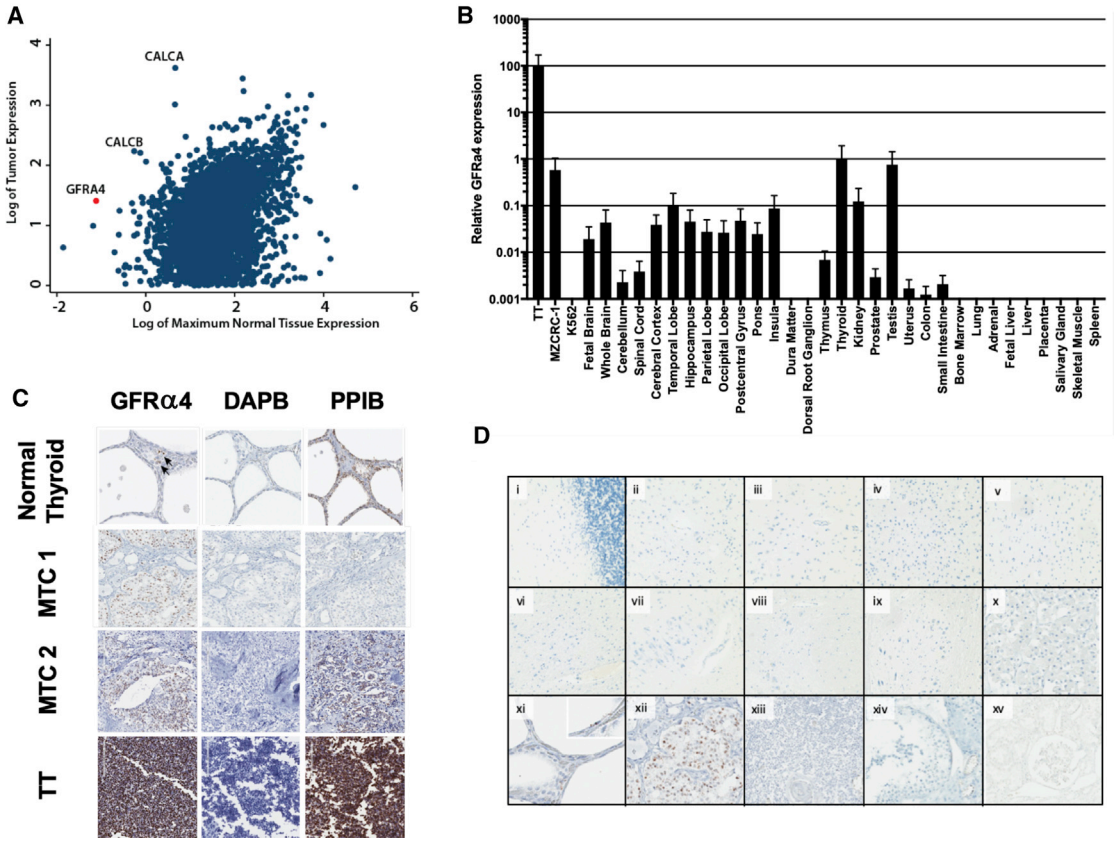

Figure 1. *GFRA4* mRNA expression in normal human tissues and MTC

(A) Log-transformed gene expression of MTC sample of index patient (y axis) is plotted against log-transformed maximum expression of genes across normal tissues (x axis). (B) Relative expression of *GFRA4* (isoforms a and b) across various human cell lines and normal tissues by qPCR with expression in thyroid set to 100. Representative data from two experiments are shown. Error bars indicate 1 standard deviation of the mean. (C) RNA *in situ* hybridization using probes against *GFRA4* (isoforms a and b), DAPB (negative control), and PPIB (positive control) in the indicated FFPE samples. Two representative examples of 7 tested MTC samples are shown. MTC 1 is from index patient. (D) RNA *in situ* hybridization with GFRα4 probes, as in (C), in the following normal human tissues or MTC: (i) cerebellum; (ii) frontal lobe; (iii) temporal lobe; (iv) occipital lobe; (v) parietal lobe; (vi) insula; (vii) hippocampus; (viii) pons; (ix) medullar; (x) pituitary; (xi) thyroid; (xii) MTC; (xiii) thymus; (xiv) testis; (xv) kidney.

In vitro evaluation of GFRα4-targeted CAR

A CAR consisting of the P4-10 variable domains with 4-1BB and CD3ζ signaling domains (P4-10bbz) (Figure 2A) was expressed on primary human T cells (Figure 2B) and a Jurkat cell line expressing an NFAT-driven GFP reporter construct. As expected, P4-10bbz-expressing Jurkat cells showed activation (i.e., expressed GFP) over basal levels in response to wells coated with GFRα4a recombinant protein but not wells coated with the other GFRα recombinant proteins (Figure 2C). We next investigated the potential for CAR activation by soluble GFRα4, given the potential existence of soluble GFRα4, either produced as secreted isoform, GFRα4c,[16] or due to shedding of the GPI-linked forms (GFRα4a and GFRα4b). Since the serum concentration of a putative soluble GFRα4 by MTC is unknown, we used recombinant human GFRα4a-Fc at concentrations above those described for other membrane-shed tumor-associated proteins that have been targeted by CAR T cells, namely mesothelin and B cell maturation antigen (BCMA), which have been detected at ng/mL concentrations in serum.[24,25] We detected no activation of P4-10bbz in reporter Jurkat cells or primary T cells by soluble GFRα4 at a concentration of 1 μg/mL and only activation of primary P4-10bbz T cells at 3 μg/mL, which is likely well above physiologic levels (Figures 2D and 2E).

P4-10bbz Jurkat cells were activated by both MTC cell lines, TT and MZ-CRC1, albeit less so by the latter, consistent with reduced *GFRA4* mRNA levels in these cells (Figure 1B). P4-10bbz CAR T cells lysed TT and MZ-CRC1 cells (Figure 3B; Figure S5) as well as K562 cells engineered to express either membrane-bound isoform of GFRα4, but not K562 cells that express other GFR family members (Figure 3B; Figures S6A, S6B, and S6D) and produced interleukin-2 (IL-2) and interferon (IFN) γ in response to cells expressing GFRα4 (Figure 3C; Figure S6C). Interestingly, P4-10bbz Jurkat cells were also activated by the neuroblastoma cell line SY5Y, which has been described to express GFRα4,[26] but were not activated by 293T cells (Figure S7).

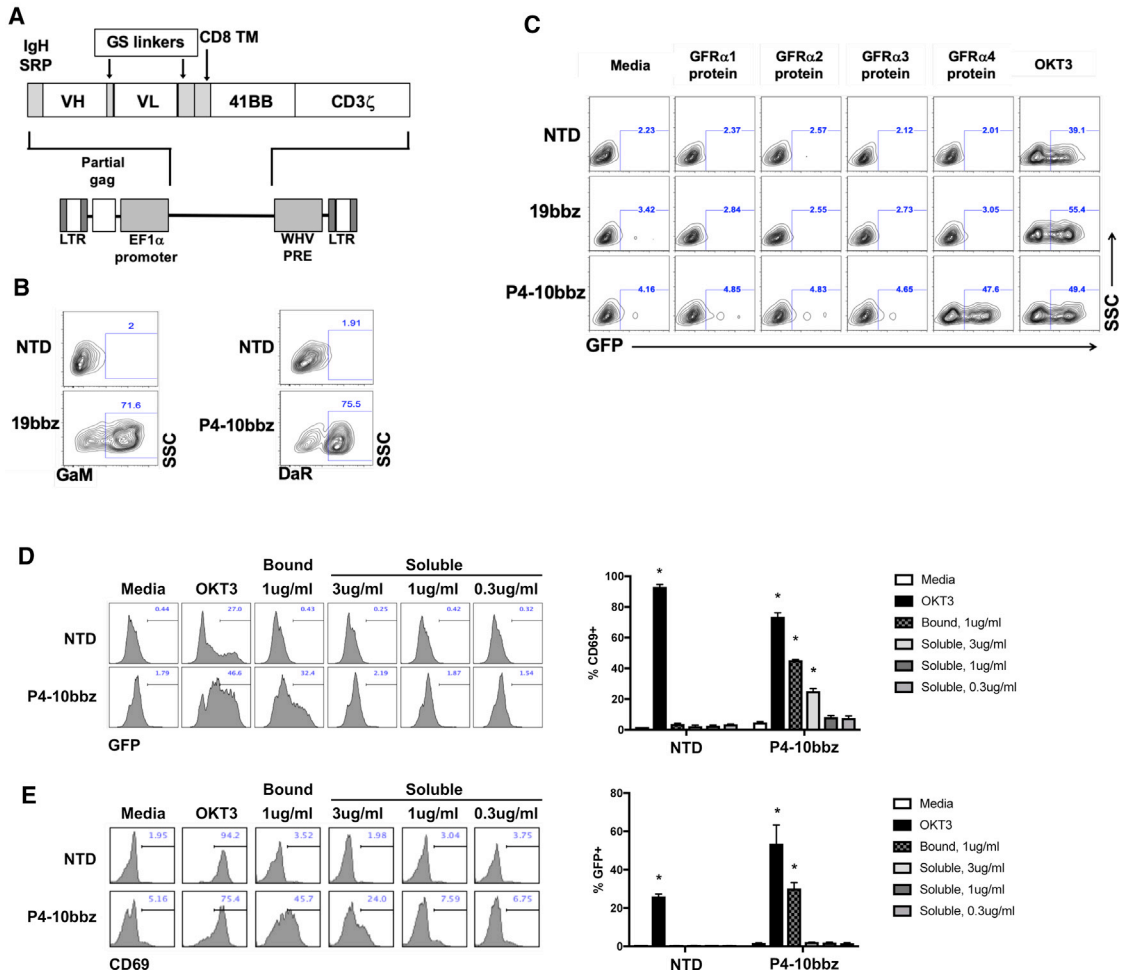

Figure 2. P4-10 CAR T cells specifically respond to GFRα4 protein *in vitro*

(A) Schematic of CAR construct inserted downstream of an EF1a-derived promoter within a 3rd-generation lentiviral vector plasmid. (B) Primary human T cells were activated using anti-CD3/anti-CD28-coated beads followed by transduction with lentiviral vectors encoding the indicated CAR genes or were left non-transduced (NTD). Seven days later, T cells were stained with biotinylated F(ab′)$_2$-specifc goat anti-mouse or donkey anti-rabbit followed by streptavidin-AF647 and analysis by flow cytometry. (C) NFAT-GFP reporter Jurkat cells expressing no CAR (NTD), 19bbz, or the P4-10bbz CAR were cultured in wells that had been coated overnight with GFRα1, GFRα2, GFRα3, GFRα4, and OKT3 proteins. Following overnight culture, cells were analyzed by flow cytometry for GFP expression. A representative of 3 independent experiments is shown. (D and E) NFAT-GFP reporter Jurkat cells (D) or primary human T cells (E) expressing no CAR (NTD), or the P4-10bbz CAR were cultured in wells that had been coated overnight with OKT3 or GFRα4 (bound) or in media with soluble GFRα4 (soluble). Following overnight culture, cells were analyzed by flow cytometry for GFP expression (*p < 0.001 compared to media control, ANOVA, Dunnett's multiple comparisons test). Representatives of 2 independent experiments each are shown. Error bars indicate 1 standard deviation of the mean.

In vivo evaluation of efficacy of GFRα4 CAR

To test P4-10bbz CAR T cells *in vivo*, we used an MTC xenograft mouse model. Click-beetle green (CBG) luciferase was expressed in TT cells, and these cells were subcutaneously implanted into non-obese diabetic severe combined immunodeficiency-gamma (NSG) mice. Mice then developed localized solid tumors that were measured by luminescence and size. P4-10bbz CAR T cells effectively eradicated tumors in this xenograft model (Figures 4A and 4B), and antitumor activity was accompanied by robust T cell expansion (Figure 4C). To compare P4-10bbz CAR T cells with an established CD19-directed CAR (19bbz) standard,[27] we ectopically expressed GFRα4b in Nalm6 cells, an acute lymphoblastic leukemia cell line that expresses CD19 (Figure S5A). 2×10^6 Nalm6-GFRα4b cells expressing CBG were purified by fluorescence-activated cell sorting (FACS), and cells were injected intravenously (i.v.) into NSG mice. Five days later, 2×10^6 CAR+ or non-CAR (NTD) T cells were injected i.v., and tumor burden was followed by luminescence imaging. Both 19bbz and P4-10bbz CAR T cells eliminated the Nalm6 signal to the limit of detection with comparable kinetics (Figure 4D). T cells in P4-10bbz-treated mice expanded more robustly compared to 19bbz-treated mice (Figure 4E), which may be related to an off-target antigen-driven stimulation (see below).

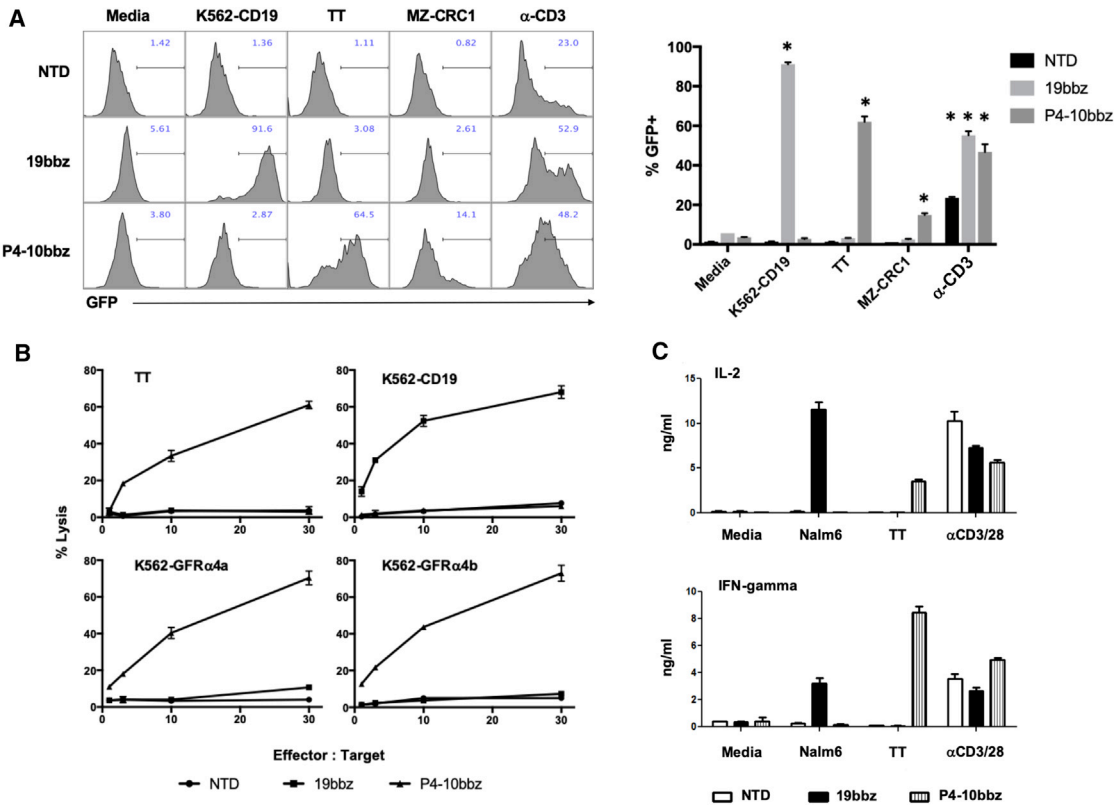

Figure 3. P4-10 CAR T cells specifically respond to GFRα4-expressing cells *in vitro*

(A) NFAT-GFP reporter Jurkat cells expressing no CAR (NTD), 19bbz, or the P4-10bbz CAR were co-cultured with the indicated stimuli overnight, followed by assessment of GFP expression in the Jurkat cells by flow cytometry (*$p < 0.05$, ANOVA, Dunnett's multiple comparisons test compared to media control). A representative of 3 independent experiments is shown. (B) Primary human T cells expressing no CAR (NTD), 19bbz, or P4-10bbz were co-cultured for approximately 18 h with ^{51}Cr-loaded TT cells or K562 cells expressing the indicated antigens, at the indicated effector:target ratios. Following co-culture, supernatant was assessed for released radioactivity. Percentage of the lysis was calculated according to the formula: 100 × (experimental − spontaneous)/(maximum − spontaneous), where spontaneous represents radioactivity released from cultures of target cells alone and maximum represents radioactivity released by target cells lysed with 5% SDS. Error bars represent 1 standard deviation of three technical replicates, and results are representative of at least 3 independent experiments. (C) Primary human T cells expressing no CAR (NTD), 19bbz, or P4-10bbz were co-cultured for 24 h with media, Nalm6 cells, TT cells, or beads coated with anti-CD3/anti-CD28 antibodies. IL-2 and IFNγ in co-culture supernatants were measured by ELISA. All error bars indicate 1 standard deviation of three technical replicates, and results are representative of at least 3 independent experiments.

Investigation of *in vivo* toxicity

Unexpectedly, in both TT and Nalm6 xenograft models, P4-10bbz-treated mice developed evidence of skin toxicity, which grossly involved the skin of the tail, footpads, and occasionally the ears (Figures 5A and 5B). Gross signs of toxicity typically became evident after tumor eradication, beginning with erythema and focal desquamation in the tail progressing to marked ulceration associated with purulent exudate. The footpads similarly developed marked ulceration and, in some mice, the outer ears became erythematous. Microscopic evaluation showed a progression from basal lymphocytic infiltration of the epidermis to marked lymphocytic interface dermatitis with basal epithelial cell apoptosis and satellitosis (Figure 5C). Lesions progressed to ulceration with epithelial necrosis covered by serocellular exudate containing coccoid bacteria (Figure 5D). Mild lymphocytic infiltration and epithelial cell apoptosis, although much less pronounced and without progression to ulceration, was also observed in stratified squamous epithelium of the middle ear, the squamous portions of the esophagus and stomach, and skin overlying other regions of the body. Other organs were normal or variably showed lymphocytic infiltration that was also seen in control T cell-treated mice (Table S3).

Many of the histologic features were reminiscent of graft-versus-host disease. Thus, although 19bbz and NTD cells were produced in parallel to P4-10bbz cells from the same healthy donor, we repeated the *in vivo* experiment using CAR T cells in which the TCR was deleted by CRISPR-Cas9 targeting TRBC (TRBCko). Additionally, we engineered TT cells to express CD19 in order to stimulate 19bbz CAR Ts *in vivo*. In contrast to continued tumor growth in mice treated with NTD T cells, TT-CD19+ tumors were eradicated with similar kinetics by 19bbz, P4-10bbz, and P4-10bbz+TRBCko CAR T cells (Figure S9A). However, only mice that received P4-10bbz or P4-10bbz+-TRBCko CAR T cells developed the toxicity, with similar kinetics (Figure S9B). In P4-10bbz+TRBCko CAR-treated mice, T cells in

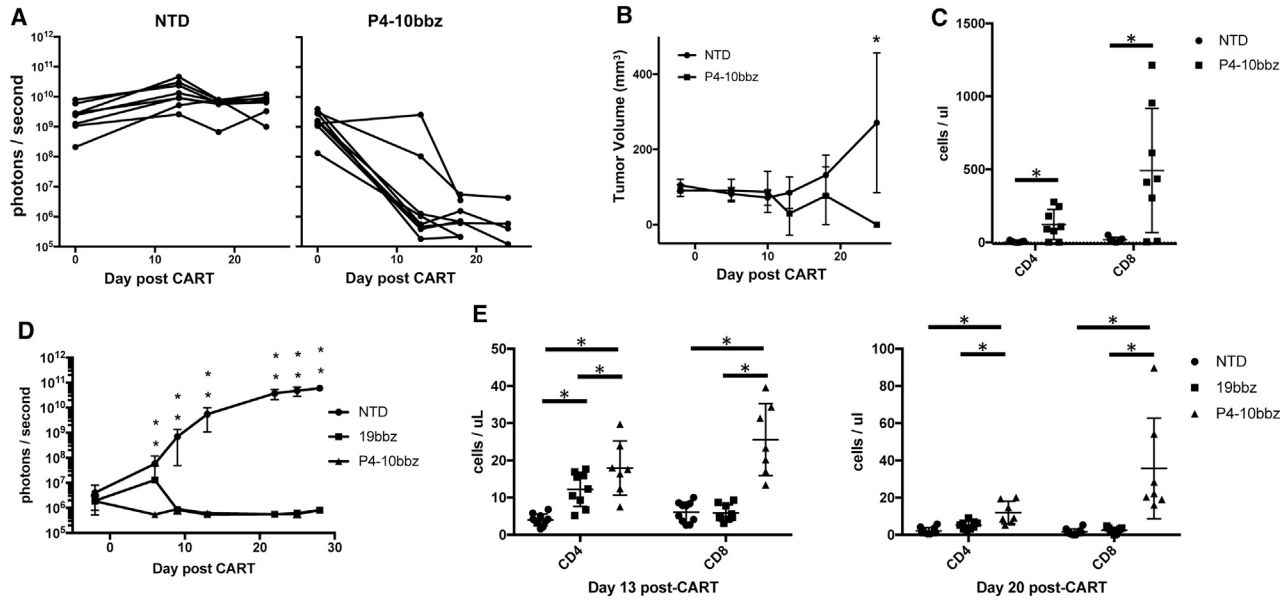

Figure 4. P4-10bbz CAR T cells control GFRα4-expressing tumors *in vivo*

(A and B) NSG mice were implanted subcutaneously with 5×10^6 TT cells engineered to express click beetle green luciferase (CBG). On day 9 post-TT cell implantation, mice received 1×10^7 T cells expressing no CAR (NTD, n = 7) or P4-10bbz (n = 8). Tumor burden was assessed by bioluminescence imaging (A) and by caliper measurement (B). Each line in (A) represents an individual mouse, and curves in (B) represent mean volumes; error bars indicate 1 standard deviation. (C) On day 21 after TT injection, peripheral blood human T cells were counted by flow cytometry (*$p < 0.05$, Student's t test). (D) NSG mice were injected intravenously with 2×10^6 Nalm6 cells engineered to express CBG and GFRα4. Five days later, mice were injected intravenously with 2×10^6 control T cells (NTD, n = 10), 19bbz (n = 10), or P4-10bbz (n = 10) CAR T cells, and tumor burden was assessed by bioluminescent imaging (*$p < 0.05$, 1-way ANOVA, Dunnett's multiple comparisons test compared to NTD). (E) On days 13 and 20 after T cell injection, peripheral blood human T cells were counted by flow cytometry (*$p < 0.05$, ANOVA, Tukey's multiple comparisons test). All error bars indicate 1 standard deviation of the mean.

the blood and infiltrating the skin remained negative for surface CD3 (Figure S10) and TCRβ (Figure S11), respectively, indicating the toxicity was TCR independent.

Thus, we focused on CAR-mediated mechanisms. Since soluble GFR family members have been reported to bind to their co-receptor, RET, *in trans*,[28,29] we hypothesized that GFRα4 released by TT cells or Nalm6-GFRα4 cells could potentially bind to RET on mouse tissue and serve as CAR targets. However, this is unlikely, since RET is expressed widely, and such a mechanism would be expected to cause more widespread tissue toxicity; additionally, we found that P4-10bbz CAR T cells caused toxicity in NSG mice even in the absence of tumors (Figure S12). To evaluate the possibility of an "on-target off-tumor" effect, we first determined whether the P4-10bbz CAR could recognize murine GFRα4. Human P4-10bbz CAR T cells did lyse K562 cells expressing mouse GFRα4 (Figure S13). However, both qPCR (Figure S14A) and RNA ISH (Figure S16) showed no evidence of *GFRA4* transcripts in mouse skin from various body regions. These data suggested that the toxicity is due to off-target reactivity. Human skin samples also demonstrated no expression of *GFRA4* mRNA by qPCR despite detection of *ACTB* indicating adequate RNA quality (Figures S14B and S14C).

To determine if the reactivity in mouse skin is relevant to human skin, we performed IHC using P4-10 expressed as a soluble full-length immunoglobulin G (IgG). Mouse skin from the tail, flank, and ears showed diffuse staining of keratinocytes (KCs) by P4-10. In contrast, human skin from 3 of 3 tested individuals showed no staining with P4-10 antibody (Figures 5E and 5F). As expected, P4-10 stained MTC and TT cells (Figure S15). Next, we functionally tested P4-10 reactivity against murine and human KCs. Jurkat cells expressing an NFAT-driven GFP reporter were transduced to express 19bbz, P4-10bbz, or PX44bbz, a positive-control CAR directed against desmoglein 1 and desmoglein 3 on murine and human KCs.[30] These CAR-reporter cells were co-cultured with K562-CD19, K562-GFRα4, and murine or human KCs cultured under in low- (0.06 mM) or high- (0.2 mM) calcium media, the latter stimulating terminal KC differentiation. After overnight co-culture, GFP and CD69 expression was measured by flow cytometry to assess CAR activation. As expected, 19bbz was activated by K562-CD19, and PX44bbz was activated by both murine and human KCs. Consistent with findings by IHC, P4-10bbz was activated by murine KCs but not by human KCs. Additionally, primary human P4-10bbz CAR T cells also did not react to human keratinocytes whereas PX44bbz CAR T cells did (Figure S17). Lastly, cytotoxicity of P4-10bbz CAR T cells was tested against a panel of primary human cells, including human keratinocytes, and showed specific lysis of only the control TT cell targets (Figure S18). Although the target antigen in mouse KCs remains unknown, the aggregate data suggest that the cross-reactive target underlying the observed toxicity in mice is likely not relevant to humans.

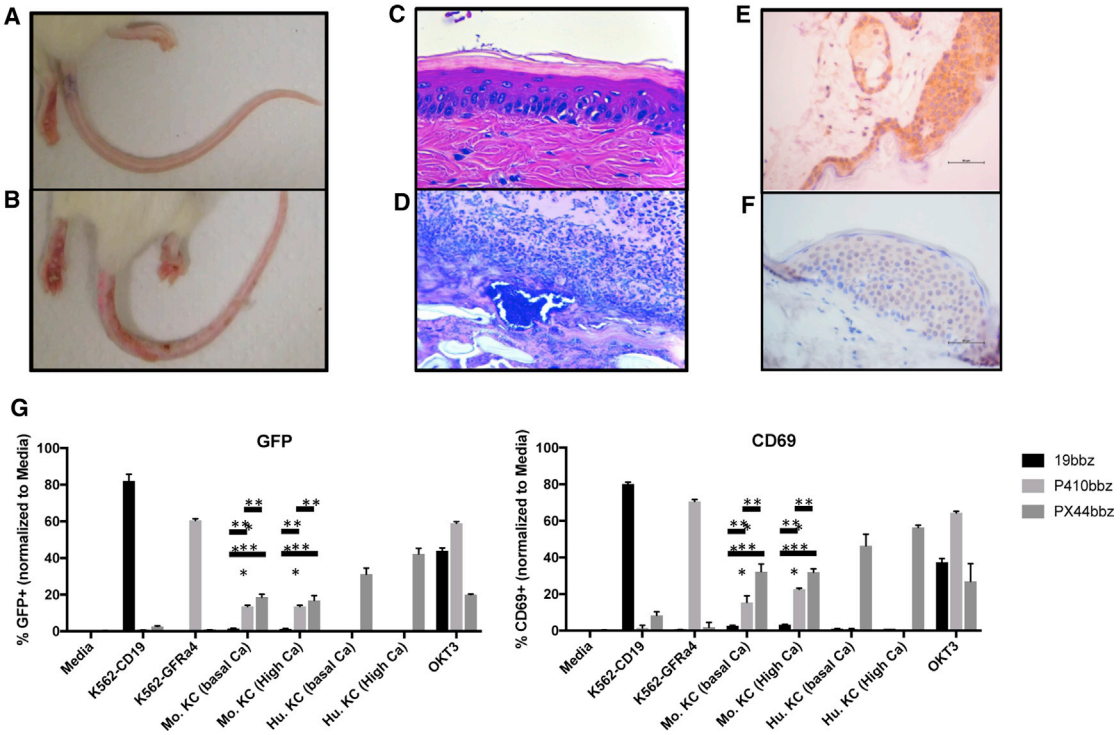

Figure 5. Skin toxicity is directed against murine but not human keratinocytes

(A) NSG mice as shown in Figure 3A implanted subcutaneously with TT cells were injected with non-CAR T cells (top) or P4-10bbz CAR T cells (bottom). (B) Hematoxylin and eosin-stained sections of tail skin from NSG mice bearing TT cell tumors followed by treatment with P4-10bbz CAR T cells prior to gross evidence of skin toxicity (top) and after ulceration (bottom). (C) Sections of skin from an NSG mouse and from a human donor stained with P4-10 antibody. (D) NFAT-GFP reporter Jurkat cells expressing 19bbz, P4-10bbz, or PX44bbz CARs were co-cultured overnight with the indicated target cells or in wells coated with the CD3-specific antibody, OKT3. Cells were then stained with a CD69-specific antibody, and GFP and CD69 expression were analyzed by flow cytometry. A representative of 2 independent experiments is shown. (**$p < 0.005$, ***$p < 0.0005$, 2-way ANOVA with Tukey's multiple comparisons test [statistics shown for Mu. KC groups only]). Mu. KC, murine keratinocytes; Hu. KC, human keratinocytes. All error bars indicate 1 standard deviation of the mean.

P4-10 humanization for clinical CAR evaluation

In order to decrease the potential immunogenicity of the rabbit-derived P4-10 scFv for use in the clinic, we humanized both the rabbit variable heavy chain (V_H) and variable light chain (V_L) domains by CDR grafting based on published methods.[31] Two new scFvs were designed and incorporated into CAR constructs, termed CAR25 and CAR29 (Figure S19). The V_L domains of both are identical and are composed of framework regions derived from the human lambda germline gene IGLV4-69*01. The V_H domains of CAR25 and CAR29 are based on human heavy chain germline framework regions of IGHV4-38-2*02 and IGHV3-48*03, respectively. Each of the 2 humanized V_H domains as well as their common V_L domain were found to have 85% amino acid sequence identity to human V_H and V_L germline genes, a level of humanization that is comparable to or greater than many humanized antibodies currently in clinical use.[32] We measured the affinity of the rabbit P4-10 and CAR29 scFvs against human GFRα4 by surface plasmon resonance (SPR); the dissociation constant (K_D) of P4-10 was 9.5×10^{-9} M and 1.14×10^{-9} M for GFRα4a and GFRα4b, respectively, and that of CAR29 was 4.87×10^{-8} M and 1.19×10^{-8} M (Figure S20). Despite a 5- to 10-fold decrease in affinity of the CAR29 scFv, we found that each of the CARs utilizing humanized P4-10 scFv was indistinguishable from the parental rabbit P4-10 CAR in terms of efficacy and specificity *in vitro* and in terms of *in vivo* efficacy and dermal toxicity (Figure S21).

DISCUSSION

We have shown that GFRα4 is a promising target for immunotherapy to treat MTC. Consistent with findings of Lindahl et al.,[16] we show, using a highly specific and sensitive RNA-ISH assay, that GFRα4 expression in humans and cynomolgus macaques is limited to parafollicular cells of the thyroid, strongly suggesting absence of protein expression. Also confirming their findings, we found GFRα4 expression in all tested cases of MTC, which derive from parafollicular cells. Others have reported GFRα4 expression in human tissues apart from the thyroid.[26,33] Using confocal imaging and sub-cellular fractionation with western blot, Lee et al.[33] reported plasma membrane expression of GFRα4 in normal human brain and mislocalization to the ER in glioma samples. However, using ISH, we were unable to detect GFRα4 mRNA in human and cynomolgus macaque brain samples from various brain regions. Using qPCR, we found GFRα4 signals from brain regions were 10- to 1,000-fold lower compared

to normal thyroid and MTC cell lines. Their study did not specify the location of brain tissue tested or the source of anti-GFRα4 antibody used.[33] The discrepancy between our findings may be due to differential sensitivity of the assays but could also be due to GFRα4 expression in an infrequent population of cells that was missed due to sampling or dilution among negative cells. Wang et al.,[26,34] investigating a potential role of GFRα4 in the pathogenesis of Hirschsprung's disease, showed decreased GFRα4 mRNA and GFRα4 protein in colonic tissue from affected subjects compared to normal individuals. However, they did not compare expression to that found in thyroid tissue.[26,34] We found no evidence of GFRα4 mRNA expression in colon, including enteric ganglia using ISH and qPCR. Additionally, the antibody used in their studies reportedly detected GFRα4 protein in 293T cells. In contrast, we found no evidence of GFRα4 expression in 293T cells when tested using our sensitive P4-10bbz CAR reporter cells (Figure 3D). Another study also investigating the potential role of GFRα4 in Hirschsprung's disease found no mutations or variants of GFRα4 associated with disease.[35] Thus, it remains unclear if GFRα4 is expressed in the colon. If it is, its expression may be at low levels or in infrequent cells.

GFRα4 is predicted to occur as two different GPI-linked membrane-bound isoforms, GFRα4a and GFRα4b, and a third soluble form, GFRα4c, although secretion of the soluble protein has yet to be demonstrated convincingly.[16] Using phage display, we constructed P4-10bbz, a CAR that targets both surface GPI-linked isoforms. We showed *in vitro* efficacy of T cells expressing P4-10bbz against target cells expressing GFRα4a or GFRα4b, but not other GFRα family members. Using a tumor xenograft model, we showed *in vivo* efficacy of P4-10bbz CAR T cells against MTC. In a model using Nalm6 cells expressing both CD19 and GFRα4, P4-10bbz CAR T cells eradicated antigen-positive tumor cells as effectively as the CD19-targeted "gold-standard" CAR T cell.

Tumor-escape due to antigen loss has been described following CAR T cell therapy in B cell malignancies.[36,37] To address the possibility of antigen loss as a mechanism of relapse in MTC, we performed small interfering RNA (siRNA)-mediated silencing of GFRα4 in TT cells and found no defect in TT cell proliferation. Thus, antigen-loss tumor escape could occur following GFRα4-targeted therapy. However, whether GFRα4-independent growth is specific to TT cells or also a feature of primary MTC cells remains to be determined. Interestingly, we found reduced expression of RET protein, but not mRNA, following GFRα4 knockdown using two different siRNAs. The reason for this is not clear but may indicate that RET is more stable when in complex with its co-receptor GFRs; loss of GFRα4 in TT cells could result in more rapid degradation of RET protein. One limitation of our study is the relatively few MTC lines available for evaluation. We tested TT and MZ-CRC1 cells, the only two MTC cell lines of which we are aware, and found that both express GFRα4 but at very different levels, for unknown reasons. Each harbors a different RET-activating mutation, and it is unknown whether this contributes to the expression level of GFRα4, a binding partner of RET.

In vivo murine studies revealed P4-10bbz CAR-mediated toxicity affecting squamous epithelia, most prominently in the skin of the tail and foot pads. The combined results of several experiments presented suggest that the toxicity is the result of off-target reactivity of the CAR to an unknown antigen found in murine but not human keratinocytes. Although a limitation of the present study is the lack of identification of the off-target antigen, we provide multiple lines of evidence to suggest its lack of relevance to humans. This underscores limitations inherent in the *in vivo* models available for evaluating CAR therapies. Future work to further evaluate the safety of GFRα4-targeted immunotherapies could employ a syngeneic CAR T model targeting murine or knocked-in human GFRα4, keeping in mind, however, that murine and human GFRα4 appear to undergo differential splicing.

In summary, we have identified and validated GFRα4 as a promising therapeutic target for treatment of MTC. We have developed a GFRα4-directed CAR T cell immunotherapy that could be an effective treatment for patients with MTC, who currently have no curative options. A clinical trial to test GFRα4-directed CAR T cells for MTC is currently under development.

MATERIALS AND METHODS

Antibodies and flow cytometry

Expression of the FMC63-based 19bbz CAR was assessed using biotin-conjugated goat anti-mouse antibody (Jackson ImmunoResearch, West Grove, PA, USA) followed by streptavidin-PE (BD Biosciences, San Jose, CA, USA) or streptavidin-APC (BD Biosciences). P4-10bbz expression was assessed by staining with biotin-conjugated donkey anti-rabbit antibody (Jackson ImmunoResearch) followed by streptavidin-PE or streptavidin-APC. Expression of GFRα4 was assessed using recombinant IgG comprising the P4-10 rabbit variable region fused to either a rabbit, mouse, or human constant region. The rabbit construct (a kind gift from Novartis) was detected by AF647-conjugated donkey anti-rabbit (Jackson ImmunoResearch), and the mouse/human constructs (constructed by WuXi AppTec, Philadelphia, PA, USA) were detected by AF647-conjugated goat anti-mouse or -human antibodies, respectively (Jackson ImmunoResearch). Expression of GFRα1, GFRα2, and GFRα3 was assessed using polyclonal rabbit anti-GFRα1, anti-GFRα2, and anti-GFRα3 (Sino Biologicals, Wayne, PA, USA) followed by AF647-conjugated goat anti-rabbit antibody (Thermo Fisher Scientific). Human T cells in mouse blood were enumerated using anti-CD3-APC-Cy7 (BD Biosciences), anti-CD4-V450 (BD Biosciences), anti-CD8-PE (BD Biosciences), anti-CD45-APC (BD Biosciences), and CountBright Absolute Counting Beads (Thermo Fisher Scientific). After a 20-min incubation, samples were fixed using BD Pharm Lyse. For analysis of Nalm6 cells in mouse blood, red blood cells were first lysed with a 5-min incubation in ACK lysis buffer (Thermo Fisher Scientific). Samples were then washed once and stained with P4-10 antibody, anti-CD3-APC-Cy7, anti-CD45-PE (BD Biosciences), and anti-CD19 (Beckman Coulter, Atlanta, GA, USA). Following a 30-min incubation and two washes, samples were stained with AF647-conjugated goat anti-rabbit antibody for 30 min. After two washes, samples

were fixed with buffered 1% paraformaldehyde. All samples were analyzed on a LSRFortessa (BD Biosciences), and data analysis was performed using FlowJo software (FlowJo).

Phage display

Antibody fragments to human GFRα4 isoform a (GFRα4a) and isoform b (GFRα4b) were isolated by phage display using a naive chimeric rabbit-human Fab M13 phage display library.[38] The library comprised >10 billion independent rabbit variable regions displayed on phage as Fab fragments with human C_{H1} heavy chain constant regions and human light chain C_κ or C_λ constant regions. Library selections against human Fc-fusion constructs of microplate-immobilized GFRα4a and GFRα4b were performed in separate experiments and carried out as described[39] in the presence of 10-fold excess soluble Fc-GFRα1, Fc-GFRα2, and Fc-GFRα3 to prevent cross-reactivity with related GDNF family alpha receptors or human Fc constant region fragments. Human GFRα1, 2, 3, and 4a were purchased from R&D Systems (Minneapolis, MN, USA), and GFRα4b was purchased from LakePharma (Belmont, CA, USA).

After four rounds of panning, individual phage-displayed Fab clones were prepared, and phage ELISA and nucleotide sequencing[39] revealed 2 unique GFRα4a- and GFRα4b-binding Fabs designated P4-6 and P4-10. Immunoglobulin sequence analysis of recombinant antibodies were performed using the IMGT tools V-Quest[40] and DomainGapAlign,[41] available at http://www.imgt.org.

SPR analysis

Kinetic and thermodynamic parameters for scFv binding to antigen were measured on a Biacore X100 instrument (Cytiva) at 25°C using 1× HBS-EP+ (Cytiva) as running buffer. A mouse anti-human IgG C_H2 monoclonal antibody (Cytiva) was immobilized on a CM5 sensor chip via standard NHS/EDC coupling methods (Cytiva) to capture the antigens hFc-GFRα4a or hFc-GFRα4b. Rabbit scFv or humanized scFv serially two-fold diluted in running buffer were then injected respectively at five different concentrations with a replicate of the lowest concentration to confirm regeneration of the sensor chip. Biacore X100 Control Software (version 2.0.1) was used to collect data and Biacore X100 Evaluation Software (version 2.0.1) to analyze data. Calculation of association (k_{on}) and dissociation (k_{off}) rate constants was based on a 1:1 Langmuir binding model. The equilibrium K_D was calculated from k_{off}/k_{on}.

CAR construction

A scFv construct was synthesized from the V_H and V_L fragments of the P4-10 Fab nucleotide sequence in V_H-V_L orientation with the 15 amino acid glycine-serine linker, GGGGSGGGGSSGGGS, between the variable domains, flanked by BamH1 and Nhe1 restriction sites (Genewiz, South Plainfield, NJ, USA). These were cloned into a lentiviral plasmid vector containing a glycine-serine hinge-domain, GGGGSGGGGS, followed by a CD8 transmembrane domain and the cytoplasmic domains of 4-1BB and CD3ζ driven by the EF1α promoter.[27] The PX44 CAR, directed to the keratinocyte adhesion molecules desmogleins 1 and 3, was similarly constructed by synthesis of the PX44 scFv[42] flanked by BamH1 and Nhe1 followed by cloning into the CAR lentivirus vector in place of the P4-10 scFv. The human CD19 directed FMC63-based CAR has been described previously.[27]

CAR T cell production

T cells were activated using anti-CD3/anti-CD28 coated Dynabeads (Thermo Fisher Scientific, Waltham, MA, USA) at a bead:cell ratio of 3:1 and cultured in RPMI1640 with 10% fetal bovine serum (FBS), 10 mM HEPES, and 1% penicillin/streptomycin. Twenty-four hours after activation, the cells were transduced with lentiviruses at a MOI of 2 to 3. T cells were then expanded in media containing 100 IU/mL IL-2 (Proleukin) for 10–14 days prior to cryopreservation or use in functional studies.

T cell receptor-deficient CAR T cells were generated by T cell activation and viral transduction as described.[43] On day 3 of culture, T cells were de-beaded and electroporated (360 V, 1 ms pulse, 2 mm gap cuvette) using an ECM 830 Square Wave Electroporation system (BTX, Holliston, MA, USA) at a concentration of 5–10 × 10^7 cells/mL in Opti-MEM with *in vitro*-transcribed Cas9 mRNA at a final concentration of 20 μg per 100 μL. Cas9 mRNA was generated from a pGEM vector encoding the Cas9 gene using mScript (Cellscript, Madison, WI, USA) following the manufacturer's recommendations. Following electroporation, T cells were returned to complete media with IL-2. On day 4, T cells were electroporated under the same conditions with *in vitro*-transcribed gRNA targeting TRBC[43] at a final concentration of 8–10 μg per 100 μL. T cells were then returned to complete media. Between days 9 and 11 of culture, TCR-positive cells were depleted using an anti-CD3 depletion kit (Miltenyi Biotec, Auburn, CA, USA). Labeled cells were serially passed through two columns over the magnet, which consistently yielded >95% surface CD3-negative cells as assessed by flow cytometry. Cells were expanded for an additional 5 days prior to cryopreservation.

Primary cells and cell lines

TT, MZ-CRC1, K562, HaCaT, and Nalm6 cells were obtained from ATCC. Jurkat cells stably expressing an NFAT-driven GFP reporter were a kind gift of Arthur Weiss (University of California, San Francisco). K562-CD19 and TT-CD19 cells were generated by transduction with a lentivirus encoding human CD19.[27] K562 cells expressing GFRα1, GFRα2, and GFRα3 were constructed by transduction with lentiviruses containing GFP followed by a T2A sequence, followed by the GFRα1/2/3 coding sequences. Nalm6 cells were transduced with a lentivirus encoding CBG luciferase and, where indicated, a lentiviral vector encoding GFRα4a or GFRα4b. All cell lines were cultured in RPMI1640 containing 10% fetal bovine serum, 10 mM HEPES, and 1% penicillin/streptomycin.

Primary human T cells, collected from healthy volunteer donors, were obtained from the Human Immunology Core at the University of Pennsylvania. Bulk T cells were isolated by negative selection using RosetteSep (StemCell Technologies, Vancouver, BC, Canada).

Human primary keratinocytes isolated from human foreskin were obtained from the University of Pennsylvania Dermatology Core. Murine keratinocytes were isolated according to a published method.[44]

NFAT-GFP Jurkat cell reporter assay

NFAT-GFP reporter Jurkat cells were engineered to express CARs by transduction with CAR-encoding lentiviral vectors. Jurkat cells were incubated overnight in the presence of indicated target cells at a 2:1 (target:Jurkat cell) ratio or in the presence of the indicated plate-bound proteins. OKT3 (10 μg/mL, Biolegend) was adsorbed onto culture wells by overnight incubation at 4°C. GFR proteins (10 μg/mL) were absorbed overnight to wells precoated with anti-human Fc (10 μg/mL).

Tumor xenograft studies

NSG (NOD.Cg-*Prkdc*^{scid} *IL2rg*^{tm1Wjl}/SzJ) mice were housed in the Stem Cell Xenograft Core Facility at the University of Pennsylvania under pathogen-free conditions. The experimental protocols were approved by the University of Pennsylvania IACUC.

In the Nalm6-GFRα4 model, 6- to 8-week-old NSG mice were injected with 2×10^6 Nalm6 cells transduced with GFRα4b and co-transduced with CBG luciferase emitting in the green spectrum (Chrom-Luc Green, Promega, Madison, WI, USA). These cells had been sorted to approximately 98% GFRα4b positivity. Cells were injected in a volume of 100 μL PBS via tail vein. On day 5, the mice were randomly assigned to study groups and injected with NTD, 19bbz CAR, or P4-10bbz CAR T cells at 2×10^6 cells in 100 μL PBS per mouse through the tail vein. Tumor burden was assessed by imaging anesthetized mice using a Xenogen Spectrum system and Living Image v4.2 software following intraperitoneal injection of 150 mg/kg D-luciferin (Caliper Life Sciences, Hopkinton, MA, USA). Each animal was imaged alone (for photon quantification) or in groups of up to 5 mice (for display purposes) in the anterior-posterior prone position at the same relative time point after luciferin injection (6 min). Data were collected until the midrange of the linear scale was reached (600–60,000 counts) or maximal exposure settings reached (f-stop 1, large binning, and 120 s), and then converted to photons/s/cm^2/steradian to normalize each image for exposure time, f-stop, binning, and animal size.

For the TT tumor model, 6- to 8-week-old mice were subcutaneously implanted with TT cells or TT cells engineered to express CD19. Tumor volume was assessed by external caliper measurement of the greatest longitudinal diameter (length) and the greatest transverse diameter (width). Tumor volume was calculated by the formula: tumor volume = 1/2(length × width^2). When tumors reached at least 100 mm^3, mice were randomly assigned to study groups and received NTD T cells or indicated CAR T cells (5×10^6) through tail vein injection.

In some experiments, TT cells transduced with CBG were injected into adult NSG mice, and tumors were assessed following CAR T cell injections by bioluminescent imaging as described above for the Nalm6 model.

Chromium release assay

Target cells were loaded with ^{51}Cr and combined with differing amounts of transduced T cells in U-bottom plates. After a 4-h incubation at 37°C, the release of free ^{51}Cr was measured using a COBRA II automated gamma-counter (Packard Instrument Company). The percent specific lysis was calculated using the formula: % specific lysis = 100 × (experimental cpm release − spontaneous cpm release)/(total cpm release − spontaneous cpm release). All data are presented as a mean ± standard deviation of triplicate wells.

Cytokine analysis

T cells were co-incubated with target cells at a 1:1 ratio or with anti-CD3/anti-CD28 beads at a 3:1 (bead:cell) ratio for 24 h. Culture supernatant was then harvested and frozen at −80°C. IFNγ and IL-2 in supernatants were measured by ELISA (R&D Systems) following the manufacturer's instructions. Data are presented as a mean ± standard deviation of triplicate wells.

qRT-PCR

RNA from a normal human tissue panel was obtained from Takara Clontech (Mountain View, CA, USA). Additionally, RNA was isolated from TT, MZ-CRC1, and K562 using the RNeasy Mini Kit (-QIAGEN, Germantown, MD, USA). RNA from human skin samples was isolated using the RNeasy Fibrous Tissue Mini Kit (QIAGEN). cDNA was synthesized using the High-Capacity RNA-to-cDNA kit from Applied Biosystems (Foster City, CA, USA). qPCR was performed using 100 ng of the cDNA per well in 20-μL reactions. Primers for GFRα4, ACTB, and RET were purchased from Applied Biosystems. Relative expression of GFRα4 and RET were calculated using the $2^{-\Delta\Delta Ct}$ method using ACTB as a reference gene.

RNA *in situ* hybridization

Chromogenic RNA *in situ* hybridization (RNAscope LS 2.5 Detection System; Advanced Cell Diagnostics, Newark, CA, USA) was performed on formalin-fixed paraffin-embedded tissue using a Leica Bond III instrument and probes to human GFRα4 (Probe-Hs-GFRA4 #417428; Advanced Cell Diagnostics). Positive (Hs-PPIB #313908; Advanced Cell Diagnostics) and negative (Hs-DapB #312038; Advanced Cell Diagnostics) control probes were used to assess RNA and tissue quality.

Immunohistochemistry

Representative samples of normal NSG mouse and human skin were investigated by immunohistochemistry using a P4-10 rabbit variable region/mouse constant region (IgG1-κ) chimeric antibody. Immunostaining was performed using a Leica BOND RXm automated platform combined with the Bond Polymer Refine Detection kit (Leica #DS9800), which allows detection of both mouse and rabbit tissue-bound IgG-based primary antibodies. This approach allowed the simultaneous detection of both the mouse and the rabbit components of the P4-10 chimeric primary antibody. For the mouse component of P4-10 antibody, isotype-matched controls were generated using the same protocol with an irrelevant mouse monoclonal primary antibody (i.e., MUM1P/IRF4, DAKO/Agilent, catalog #M7259)

incubated at the same concentration of the P4-10 antibody (15 μg/mL). For the rabbit component of P4-10 chimeric antibody, the rabbit anti-mouse IgG antibody linker present in the kit served as isotype control. Subcutaneous xenografts generated in NSG mice transplanted with TT cells (ATCC CRL-1803) were used as positive controls.

For immunohistochemistry, 5-μm-thick paraffin sections were mounted on ProbeOn slides (Thermo Fisher Scientific). Briefly, after dewaxing and rehydration, sections were pretreated with the epitope retrieval BOND ER1 low pH buffer (Leica #AR9961) for 20 min at 98°C. Endogenous peroxidase was inactivated with 3% H_2O_2 for 10 min at room temperature (RT). Nonspecific tissue-antibody interactions were blocked with Leica PowerVision IHC/ISH Super Blocking solution (PV6122) for 30 min at RT. The same blocking solution also served as diluent for the primary antibody. Immunoreactivity was revealed with the diaminobenzidine (DAB) chromogen reaction. Slides were finally counterstained in hematoxylin, dehydrated in an ethanol series, cleared in xylene, and permanently mounted with a resinous mounting medium (Thermo Fisher Scientific ClearVue coverslipper).

RET and GFRα4 knockdown

TT cells that were engineered to express GFP were electroporated with siRNA oligonucleotides (Integrated DNA Technologies, Coralville, IA, USA) targeting GFP (positive control), RET, GFRα4, or with a non-targeting siRNA (negative control). Twenty-four hours later, cells were lysed, and mRNA was isolated for measurement of RET and GFRα4 by qPCR. Cells were also maintained in culture and counted 7 days later to assess proliferation.

Statistical analysis

Statistical analyses, as indicated in figure legends, were performed using Prism (GraphPad Software, San Diego, CA, USA).

Data and materials availability

Plasmids and lentiviral vectors encoding the scFvs and CARs as well as cell lines described in this manuscript are available to interested investigators, but their availability will depend upon the execution of a material transfer agreement with the University of Pennsylvania.

SUPPLEMENTAL INFORMATION

Supplemental information can be found online at https://doi.org/10.1016/j.omto.2021.01.012.

ACKNOWLEDGMENTS

The authors thank Roger B. Cohen, MD, for critical review of this manuscript, Xiaowei Xu, MD, PhD, for advice related to toxicity evaluation, Daniel Martinez and Amy Ziober for assistance with immunohistochemistry and RNAscope studies, and Jiangtao Ren, PhD, and Yangbing Zhao, PhD, for assistance with TRBC deletion using CRISPR/Cas9. The work presented was funded through the REACT Thyroid Foundation and Tmunity Therapeutics, with additional support from Novartis. V.G.B. is funded by the Burroughs Wellcome Fund.

AUTHOR CONTRIBUTIONS

V.G.B. conceived, designed, and performed experiments; analyzed data; and wrote the manuscript. L.L., S.K., D.A., K.Z., Z.Z., S.N.C., G.G., E.R., K.M., and M.D.F. assisted with experiments and data analysis. R.S.G., H.P., and C.R. supported antibody discovery and development. D.L.S. conceived, designed, and performed experiments; analyzed data; and edited the manuscript. M.C.M. conceived and designed experiments, analyzed data, and wrote the manuscript.

DECLARATION OF INTERESTS

D.L.S., V.G.B., C.R., R.S.G., and M.C.M. have filed a patent application on technology presented in this manuscript.

REFERENCES

1. Pacini, F., Castagna, M.G., Cipri, C., and Schlumberger, M. (2010). Medullary thyroid carcinoma. Clin. Oncol. (R. Coll. Radiol.) *22*, 475–485.
2. Roy, M., Chen, H., and Sippel, R.S. (2013). Current understanding and management of medullary thyroid cancer. Oncologist *18*, 1093–1100.
3. Ernani, V., Kumar, M., Chen, A.Y., and Owonikoko, T.K. (2016). Systemic treatment and management approaches for medullary thyroid cancer. Cancer Treat. Rev. *50*, 89–98.
4. Schlumberger, M., Carlomagno, F., Baudin, E., Bidart, J.M., and Santoro, M. (2008). New therapeutic approaches to treat medullary thyroid carcinoma. Nat. Clin. Pract. Endocrinol. Metab. *4*, 22–32.
5. Klein Hesselink, E.N., Steenvoorden, D., Kapiteijn, E., Corssmit, E.P., van der Horst-Schrivers, A.N., Lefrandt, J.D., Links, T.P., and Dekkers, O.M. (2015). Therapy of endocrine disease: response and toxicity of small-molecule tyrosine kinase inhibitors in patients with thyroid carcinoma: a systematic review and meta-analysis. Eur. J. Endocrinol. *172*, R215–R225.
6. Elisei, R., Schlumberger, M.J., Müller, S.P., Schöffski, P., Brose, M.S., Shah, M.H., Licitra, L., Jarzab, B., Medvedev, V., Kreissl, M.C., et al. (2013). Cabozantinib in progressive medullary thyroid cancer. J. Clin. Oncol. *31*, 3639–3646.
7. Wells, S.A., Jr., Robinson, B.G., Gagel, R.F., Dralle, H., Fagin, J.A., Santoro, M., Baudin, E., Elisei, R., Jarzab, B., Vasselli, J.R., et al. (2012). Vandetanib in patients with locally advanced or metastatic medullary thyroid cancer: a randomized, double-blind phase III trial. J. Clin. Oncol. *30*, 134–141.
8. Milone, M.C., and Bhoj, V.G. (2018). The Pharmacology of T Cell Therapies. Mol. Ther. Methods Clin. Dev. *8*, 210–221.
9. Bhoj, V.G., Arhontoulis, D., Wertheim, G., Capobianchi, J., Callahan, C.A., Ellebrecht, C.T., Obstfeld, A.E., Lacey, S.F., Melenhorst, J.J., Nazimuddin, F., et al. (2016). Persistence of long-lived plasma cells and humoral immunity in individuals responding to CD19-directed CAR T-cell therapy. Blood *128*, 360–370.
10. Maude, S.L., Laetsch, T.W., Buechner, J., Rives, S., Boyer, M., Bittencourt, H., Bader, P., Verneris, M.R., Stefanski, H.E., Myers, G.D., et al. (2018). Tisagenlecleucel in Children and Young Adults with B-Cell Lymphoblastic Leukemia. N. Engl. J. Med. *378*, 439–448.
11. Schuster, S.J., Bishop, M.R., Tam, C.S., Waller, E.K., Borchmann, P., McGuirk, J.P., Jäger, U., Jaglowski, S., Andreadis, C., Westin, J.R., et al.; JULIET Investigators (2019). Tisagenlecleucel in Adult Relapsed or Refractory Diffuse Large B-Cell Lymphoma. N. Engl. J. Med. *380*, 45–56.
12. Knochelmann, H.M., Smith, A.S., Dwyer, C.J., Wyatt, M.M., Mehrotra, S., and Paulos, C.M. (2018). CAR T Cells in Solid Tumors: Blueprints for Building Effective Therapies. Front. Immunol. *9*, 1740.
13. Wei, J., Han, X., Bo, J., and Han, W. (2019). Target selection for CAR-T therapy. J. Hematol. Oncol. *12*, 62.

14. Lamers, C.H., Sleijfer, S., van Steenbergen, S., van Elzakker, P., van Krimpen, B., Groot, C., Vulto, A., den Bakker, M., Oosterwijk, E., Debets, R., and Gratama, J.W. (2013). Treatment of metastatic renal cell carcinoma with CAIX CAR-engineered T cells: clinical evaluation and management of on-target toxicity. Mol. Ther. *21*, 904–912.

15. Airaksinen, M.S., Titievsky, A., and Saarma, M. (1999). GDNF family neurotrophic factor signaling: four masters, one servant? Mol. Cell. Neurosci. *13*, 313–325.

16. Lindahl, M., Poteryaev, D., Yu, L., Arumae, U., Timmusk, T., Bongarzone, I., Aiello, A., Pierotti, M.A., Airaksinen, M.S., and Saarma, M. (2001). Human glial cell line-derived neurotrophic factor receptor alpha 4 is the receptor for persephin and is predominantly expressed in normal and malignant thyroid medullary cells. J. Biol. Chem. *276*, 9344–9351.

17. Lindfors, P.H., Lindahl, M., Rossi, J., Saarma, M., and Airaksinen, M.S. (2006). Ablation of persephin receptor glial cell line-derived neurotrophic factor family receptor alpha4 impairs thyroid calcitonin production in young mice. Endocrinology *147*, 2237–2244.

18. Felsenfeld, A.J., and Levine, B.S. (2015). Calcitonin, the forgotten hormone: does it deserve to be forgotten? Clin. Kidney J. *8*, 180–187.

19. Mundy, G.R., and Guise, T.A. (1999). Hormonal control of calcium homeostasis. Clin. Chem. *45*, 1347–1352.

20. Bongarzone, I., Vigano, E., Alberti, L., Mondellini, P., Uggeri, M., Pasini, B., Borrello, M.G., and Pierotti, M.A. (1999). The Glu632-Leu633 deletion in cysteine rich domain of Ret induces constitutive dimerization and alters the processing of the receptor protein. Oncogene *18*, 4833–4838.

21. The Human Protein Atlas. GFRA4. https://www.proteinatlas.org/search/gfra4.

22. Lian, E.Y., Maritan, S.M., Cockburn, J.G., Kasaian, K., Crupi, M.J., Hurlbut, D., Jones, S.J., Wiseman, S.M., and Mulligan, L.M. (2017). Differential roles of RET isoforms in medullary and papillary thyroid carcinomas. Endocr. Relat. Cancer *24*, 53–69.

23. Koga, K., Hattori, Y., Komori, M., Narishima, R., Yamasaki, M., Hakoshima, M., Fukui, T., and Maitani, Y. (2010). Combination of RET siRNA and irinotecan inhibited the growth of medullary thyroid carcinoma TT cells and xenografts via apoptosis. Cancer Sci. *101*, 941–947.

24. Hassan, R., Remaley, A.T., Sampson, M.L., Zhang, J., Cox, D.D., Pingpank, J., Alexander, R., Willingham, M., Pastan, I., and Onda, M. (2006). Detection and quantitation of serum mesothelin, a tumor marker for patients with mesothelioma and ovarian cancer. Clin. Cancer Res. *12*, 447–453.

25. Chen, H., Li, M., Xu, N., Ng, N., Sanchez, E., Soof, C.M., Patil, S., Udd, K., Bujarski, S., Cao, J., et al. (2019). Serum B-cell maturation antigen (BCMA) reduces binding of anti-BCMA antibody to multiple myeloma cells. Leuk. Res. *81*, 62–66.

26. Wang, G., Guo, F., Wang, H., Liu, W., Zhang, L., Cui, M., and Wu, X. (2017). Downregulation of microRNA-483-5p Promotes Cell Proliferation and Invasion by Targeting GFRA4 in Hirschsprung's Disease. DNA Cell Biol. *36*, 930–937.

27. Milone, M.C., Fish, J.D., Carpenito, C., Carroll, R.G., Binder, G.K., Teachey, D., Samanta, M., Lakhal, M., Gloss, B., Danet-Desnoyers, G., et al. (2009). Chimeric receptors containing CD137 signal transduction domains mediate enhanced survival of T cells and increased antileukemic efficacy in vivo. Mol. Ther. *17*, 1453–1464.

28. Paratcha, G., Ledda, F., Baars, L., Coulpier, M., Besset, V., Anders, J., Scott, R., and Ibáñez, C.F. (2001). Released GFRalpha1 potentiates downstream signaling, neuronal survival, and differentiation via a novel mechanism of recruitment of c-Ret to lipid rafts. Neuron *29*, 171–184.

29. Yang, J., Runeberg-Roos, P., Leppänen, V.M., and Saarma, M. (2007). The mouse soluble GFRalpha4 receptor activates RET independently of its ligand persephin. Oncogene *26*, 3892–3898.

30. Ellebrecht, C.T., Bhoj, V.G., Nace, A., Choi, E.J., Mao, X., Cho, M.J., Di Zenzo, G., Lanzavecchia, A., Seykora, J.T., Cotsarelis, G., et al. (2016). Reengineering chimeric antigen receptor T cells for targeted therapy of autoimmune disease. Science *353*, 179–184.

31. Goydel RS, Weber J, Peng H, Qi J, Soden J, Freeth J, Park H, Rader C.J Biol Chem. 2020 May 1;295(18):5995-6006. doi: 10.1074/jbc.RA120.012791.

32. Mayrhofer, P., and Kunert, R. (2019). Nomenclature of humanized mAbs: Early concepts, current challenges and future perspectives. Hum. Antibodies *27*, 37–51.

33. Lee, K., Byun, K., Hong, W., Chuang, H.Y., Pack, C.G., Bayarsaikhan, E., Paek, S.H., Kim, H., Shin, H.Y., Ideker, T., and Lee, B. (2013). Proteome-wide discovery of mislocated proteins in cancer. Genome Res. *23*, 1283–1294.

34. Wang, G., Zhang, L., Wang, H., Cui, M., Liu, W., Liu, Y., and Wu, X. (2018). Demethylation of GFRA4 Promotes Cell Proliferation and Invasion in Hirschsprung Disease. DNA Cell Biol. *37*, 316–324.

35. Borrego, S., Fernández, R.M., Dziema, H., Niess, A., López-Alonso, M., Antiñolo, G., and Eng, C. (2003). Investigation of germline GFRA4 mutations and evaluation of the involvement of GFRA1, GFRA2, GFRA3, and GFRA4 sequence variants in Hirschsprung disease. J. Med. Genet. *40*, e18.

36. Orlando, E.J., Han, X., Tribouley, C., Wood, P.A., Leary, R.J., Riester, M., Levine, J.E., Qayed, M., Grupp, S.A., Boyer, M., et al. (2018). Genetic mechanisms of target antigen loss in CAR19 therapy of acute lymphoblastic leukemia. Nat. Med. *24*, 1504–1506.

37. Pillai, V., Muralidharan, K., Meng, W., Bagashev, A., Oldridge, D.A., Rosenthal, J., Van Arnam, J., Melenhorst, J.J., Mohan, D., DiNofia, A.M., et al. (2019). CAR T-cell therapy is effective for CD19-dim B-lymphoblastic leukemia but is impacted by prior blinatumomab therapy. Blood Adv. *3*, 3539–3549.

38. Peng, H., Nerreter, T., Chang, J., Qi, J., Li, X., Karunadharma, P., Martinez, G.J., Fallahi, M., Soden, J., Freeth, J., et al. (2017). Mining Naïve Rabbit Antibody Repertoires by Phage Display for Monoclonal Antibodies of Therapeutic Utility. J. Mol. Biol. *429*, 2954–2973.

39. Rader, C., Steinberger, P., and Barbas, C.F., III (2001). Chapter 10. Selection from Antibody Libraries; Chapter 11. Analysis of Selected Antibodies. In Phage Display: A Laboratory Manual, C.F. Barbas, III, D.R. Burton, J.K. Scott, and G.J. Silverman, eds. (Cold Spring Harbor Laboratory Press), pp. 10.11–10.20; 11.11–11.24.

40. Brochet, X., Lefranc, M.P., and Giudicelli, V. (2008). IMGT/V-QUEST: the highly customized and integrated system for IG and TR standardized V-J and V-D-J sequence analysis. Nucleic Acids Res. *36*, W503–W508.

41. Ehrenmann, F., Kaas, Q., and Lefranc, M.P. (2010). IMGT/3Dstructure-DB and IMGT/DomainGapAlign: a database and a tool for immunoglobulins or antibodies, T cell receptors, MHC, IgSF and MhcSF. Nucleic Acids Res. *38*, D301–D307.

42. Payne, A.S., Ishii, K., Kacir, S., Lin, C., Li, H., Hanakawa, Y., Tsunoda, K., Amagai, M., Stanley, J.R., and Siegel, D.L. (2005). Genetic and functional characterization of human pemphigus vulgaris monoclonal autoantibodies isolated by phage display. J. Clin. Invest. *115*, 888–899.

43. Ren, J., Zhang, X., Liu, X., Fang, C., Jiang, S., June, C.H., and Zhao, Y. (2017). A versatile system for rapid multiplex genome-edited CAR T cell generation. Oncotarget *8*, 17002–17011.

44. Li, F., Adase, C.A., and Zhang, L.J. (2017). Isolation and Culture of Primary Mouse Keratinocytes from Neonatal and Adult Mouse Skin. J. Vis. Exp. *125*, 56027.

OMTO, Volume *20*

Supplemental Information

Adoptive T cell immunotherapy for medullary thyroid carcinoma targeting GDNF family receptor alpha 4

Vijay G. Bhoj, Lucy Li, Kalpana Parvathaneni, Zheng Zhang, Stephen Kacir, Dimitrios Arhontoulis, Kenneth Zhou, Bevin McGettigan-Croce, Selene Nunez-Cruz, Gayathri Gulendran, Alina C. Boesteanu, Laura Johnson, Michael D. Feldman, Enrico Radaelli, Keith Mansfield, MacLean Nasrallah, Rebecca S. Goydel, Haiyong Peng, Christoph Rader, Michael C. Milone, and Don L. Siegel

Supplemental Materials:

Table S1. Raw data (Ct values) corresponding to Figure 1b.

Cell / Tissue	Ct values (ACTB)					Ct values (GFRa4)					Mean Ct (ACTB)	Mean Ct (GFRa4)
TT	20.93	20.93	20.95	20.94	26.79	25.69	25.74	25.88	20.9375	26.025		
MZCRC-1	16.88	17.07	17.04	17.06	30.01	29.33	29.3	29.65	17.0125	29.5725		
K562	16.6	16.67	16.6	16.58	Not Detected				16.6125	Not Detected		
Fetal Brain	19.17	19.01	19.12	19.19	36.65	36.62	36.88	36.29	19.1225	36.61		
Whole Brain	18.38	18.3	18.37	18.35	34.5	34.98	34.63	34.53	18.35	34.66		
Cerebellum	19.16	19.14	19.11	19.14	40	39.2	39.61	40	19.1375	39.7025		
Spinal Cord	19.72	19.73	19.71	19.78	38.81	40	39.37	40	19.735	39.545		
Cerebral Cortex	18.32	18.38	18.37	18.39	35.82	34.55	34.73	34.25	18.365	34.8375		
Temporal Lobe	18.61	18.62	18.53	18.6	33.85	33.54	33.99	33.37	18.59	33.6875		
Hippocampus	18.73	18.83	18.77	18.9	34.66	34.81	35.51	35.21	18.8075	35.0475		
Parietal Lobe	19.12	18.98	19.03	19.01	35.68	35.75	36.34	36.22	19.035	35.9975		
Occipital Lobe	19.29	19.29	19.28	19.23	36.61	36.46	35.93	36.27	19.2725	36.3175		
Postcentral Gyrus	19.64	19.66	19.65	19.68	35.84	35.91	35.47	36.16	19.6575	35.845		
Pons	19.1	19.03	19.04	19.01	36.61	35.63	36.03	36.43	19.045	36.175		
Insula	19.78	19.77	19.75	19.8	34.94	35.25	34.91	35.21	19.775	35.0775		
Dura Matter	17.58	17.56	17.56	17.56	Not Detected				17.565	Not Detected		
Dorsal Root Ganglion	19.8	19.84	19.82	20.05	Not Detected				19.8775	Not Detected		
Thymus	17.83	17.81	17.79	17.87	38.04	36.45	36.79	35.91	17.825	36.7975		
Thyroid	19.96	19.92	19.95	20.01	31.67	31.89	31.61	31.76	19.96	31.7325		
Kidney	19.83	19.78	19.8	19.83	34.42	34.7	34.76	34.58	19.81	34.615		
Prostate	18.9	18.86	18.87	18.87	40	Not Detected	39.21	38.02	18.875	39.07666667		
Testis	19.03	19.07	18.99	18.99	31.1	31.07	31.34	31.31	19.02	31.205		
Uterus	18.13	18.19	18.2	18.13	39.29	Not Detected	40	38.25	18.1625	39.18		
Colon	18.08	18.15	18.18	18.13	38.71	40	Not Detected	40	18.135	39.57		
Small Intestine	18.58	18.41	18.58	18.58	38.22	40	38.74	40	18.5375	39.24		
Bone Marrow	19.07	19.15	19.14	19.2	Not Detected				19.14	Not Detected		
Lung	18.53	18.57	18.52	18.55	Not Detected				18.5425	Not Detected		
Adrenal	19.26	19.49	19.46	19.54	Not Detected				19.4375	Not Detected		
Fetal Liver	18.89	18.9	18.9	18.9	Not Detected				18.8975	Not Detected		
Liver	22.24	22.16	22.22	22.22	Not Detected				22.21	Not Detected		
Placenta	20.79	20.8	20.7	20.7	Not Detected				20.7475	Not Detected		
Salivary Gland	20.71	21.24	21.21	21.31	Not Detected				21.1175	Not Detected		
Skeletal Muscle	20.73	20.73	20.75	21.27	Not Detected				20.87	Not Detected		
Spleen	18.99	18.99	19.08	19.08	Not Detected				19.035	Not Detected		

Table S2. Summary of *GFRA4* mRNA expression analysis by in-situ hybridization. FFPE samples of the indicated tissues were analyzed by in situ hybridization (RNAscope) with probes targeting human or cynomolgus macaque GFRα4. Positive and negative control probes to PPIB and DapB were tested in parallel for each experimental run. Results of qualitative analysis is shown. N/A, not applicable; N/T, not tested

Tissue	**Human**	**Cynomolgus Macaque**
MTC	+	N/A
TT cell line	+	N/A
Thyroid	+	+
Parathyroid	-	-
Adrenal	-	-
Pituitary	-	-
Ovary	-	-
Thymus	-	-
Pancreas	-	N/T
Esophagus	-	N/T
Stomach	-	N/T
Liver	-	N/T
Small Bowel	-	N/T
Colon	-	N/T
Urinary Bladder	-	-
Testis	-	N/T
Cerebellum	-	-
Cerebral Cortex	-	-
Temporal lobe	-	
Frontal lobe	-	
Occipital lobe	-	
Insula	-	N/T
Pons	-	-
Hippocampus	-	N/T
Medulla	-	N/T
Spinal cord	-	-

Table S3. Summary of toxicity in P4-10 CAR T cell treated mice. NSG mice bearing TT cell tumors were treated with P4-10bbz CAR T cells and were euthanized between 2-3 weeks after T cell injection, and animals were subjected to necropsy including gross and microscopic evaluation.

* Compared to non-CAR and 19bbz CAR T cell treated mice.

Organs without lesion*	**Affected Organs**
Heart	Stomach
Skeletal muscle	Skin
Salivary glands	Oral cavity/upper esophagus (portion with squamous epithelium)
Lower esophagus	
Trachea	
Lung	
Liver	
Gall bladder	
Spleen	
Kidneys	
Adrenal glands	
Cecum	
Small intestine	
Large intestine	
Pancreas	
Mesentery	
Mesenteric lymph nodes	
Testicles, epididymis	
Vas deferens	
Prostate gland, ampulla	
Seminal vesicles	
Preputial glands	
Urinary bladder	
Bone marrow	
Brain	
Thyroid glands	

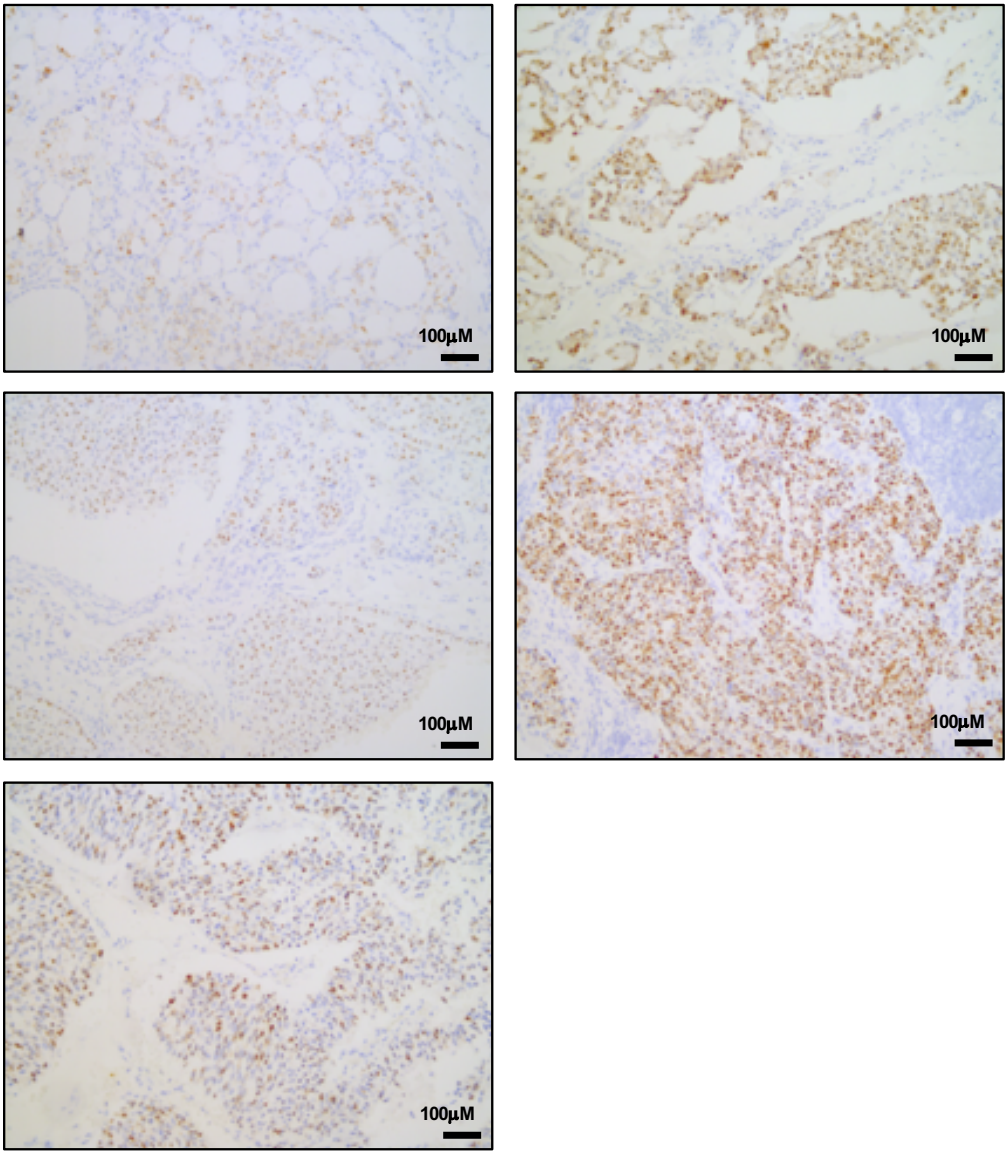

Figure S1: *GFRA4* mRNA in situ hybridization reveals expression in MTC. Five cases of MTC were tested by RNA in situ hybridization (RNAscope) using probes specific to *GFRA4*.

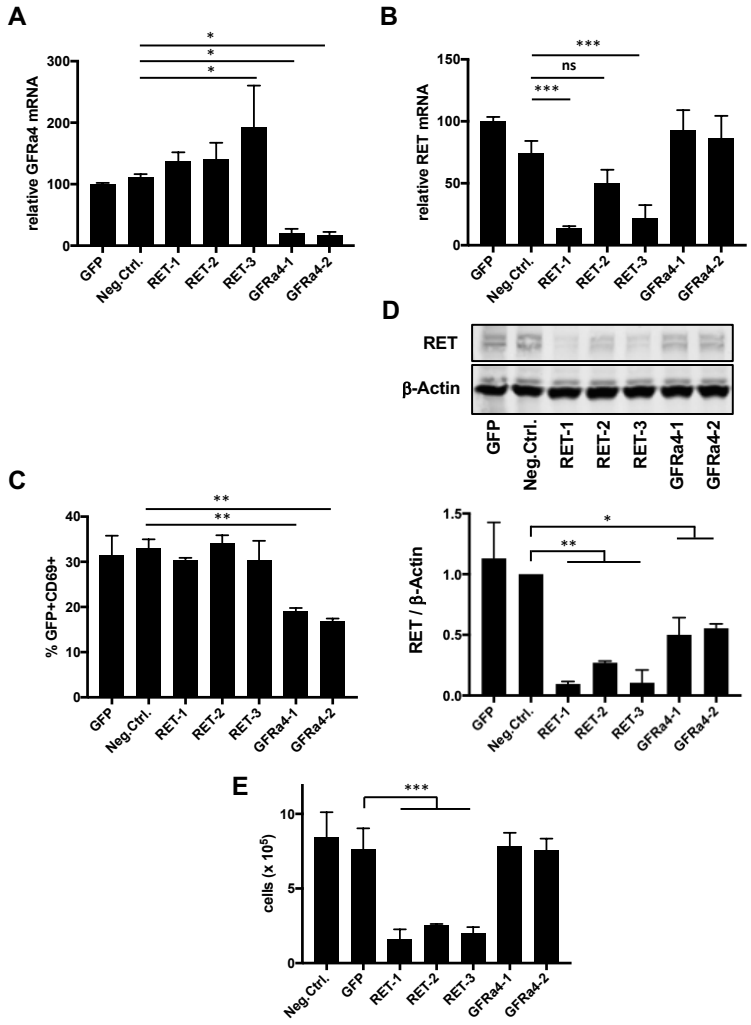

Figure S2: RET but not GFRα4 is required for TT cell proliferation. 2 x 10^5 TT cells expressing GFP were electroporated with siRNAs targeting GFP, RET, GFRα4 or a non-targeting siRNA (Neg. Ctrl.). 24-hours later, GFRα4 **(A)** and RET **(B)** mRNA was measured by qPCR. **(C)** GFRα4 protein level was functionally assessed by co-culture with NFAT-GFP reporter Jurkat cells expressing the GFRα4-specific CAR, P4-10bbz, and upregulation of GFP and CD69 was assessed as an indication of surface GFRα4 expression. **(D)** RET protein expression was determined by western blot. **(E)** Seven days after siRNA electroporation, cells were counted to determine survival/proliferation. Error bars indicate standard deviation. (* $p<0.05$,** $p<0.005$, *** $p<0.0005$, One-way ANOVA with Dunnett's multiple comparisons test).

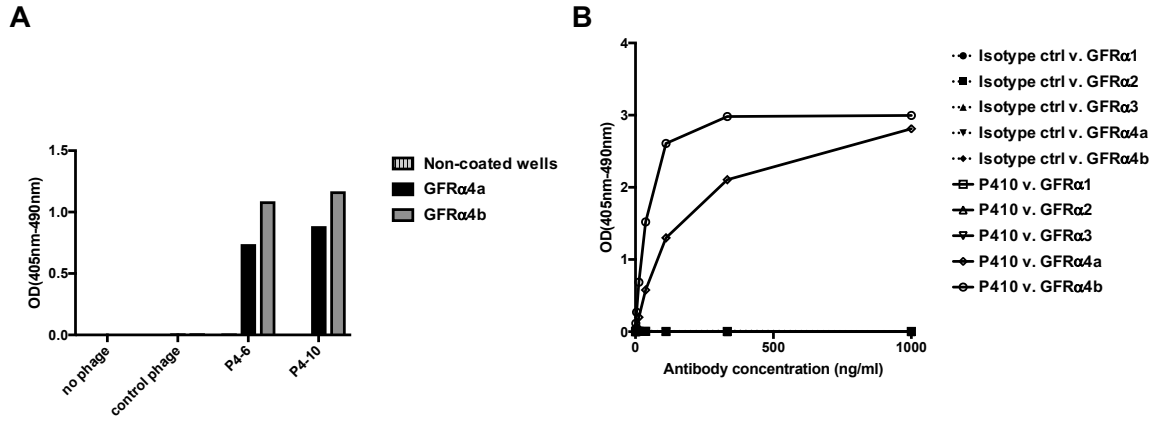

Figure S3: Binding specificities of P4-6 and P4-10 antibodies to GFRα proteins. (A) Phage ELISA of P4-6 and P4-10 rabbit/human chimeric Fab fragments binding to immobilized GFRα4a and GFRα4b proteins. Control phage is phage-displayed isotype control rabbit/human γλ Fab fragment; (B) ELISA of full-length rabbit/murine chimeric IgG binding to GFRα1, GFRα2, GFRα3, GFRα4a, and GFRα4b proteins.

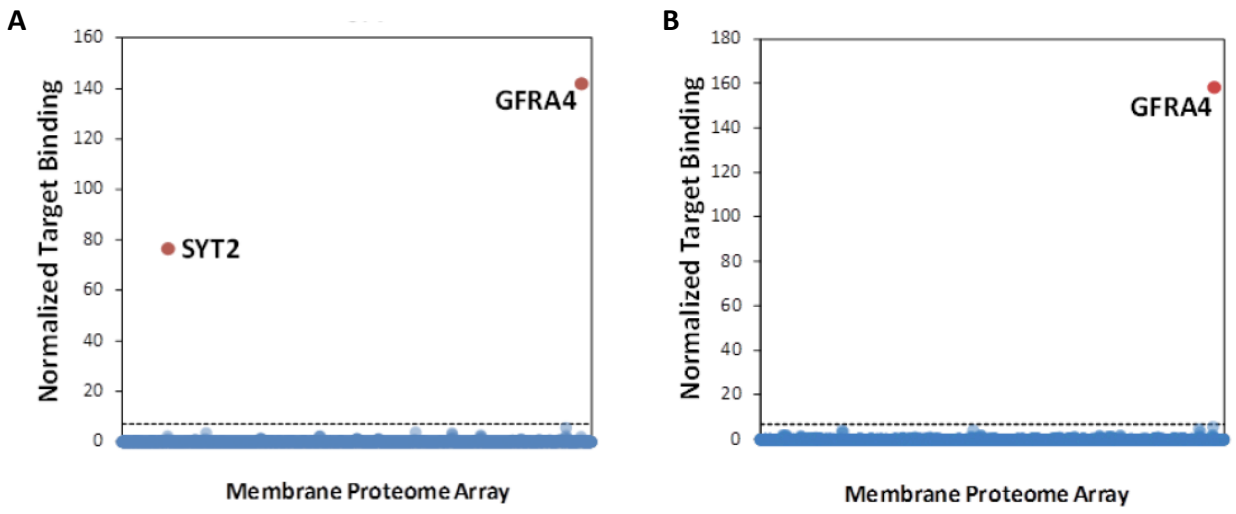

Figure S4. Identification of membrane protein binding targets for P4-6 and P4-10. A Membrane Proteome Array (MPA) was probed with P4-6 (A) and P4-10 (B) Fab proteins followed by detection using a fluorescently-labeled secondary antibody. Fluorescence readings from each experimental plate were validated using positive (construct expressing GFRα4) and negative (empty vector) controls. Binding values for each individual membrane protein target were normalized and transformed to give a single numerical value for binding of the antibody against each target protein (Normalized Target Binding). Non-specific fluorescence was determined to be any value below 3 standard deviations above noise (dotted line). Targets that showed increased antibody binding are displayed above the dotted line and denoted in red.

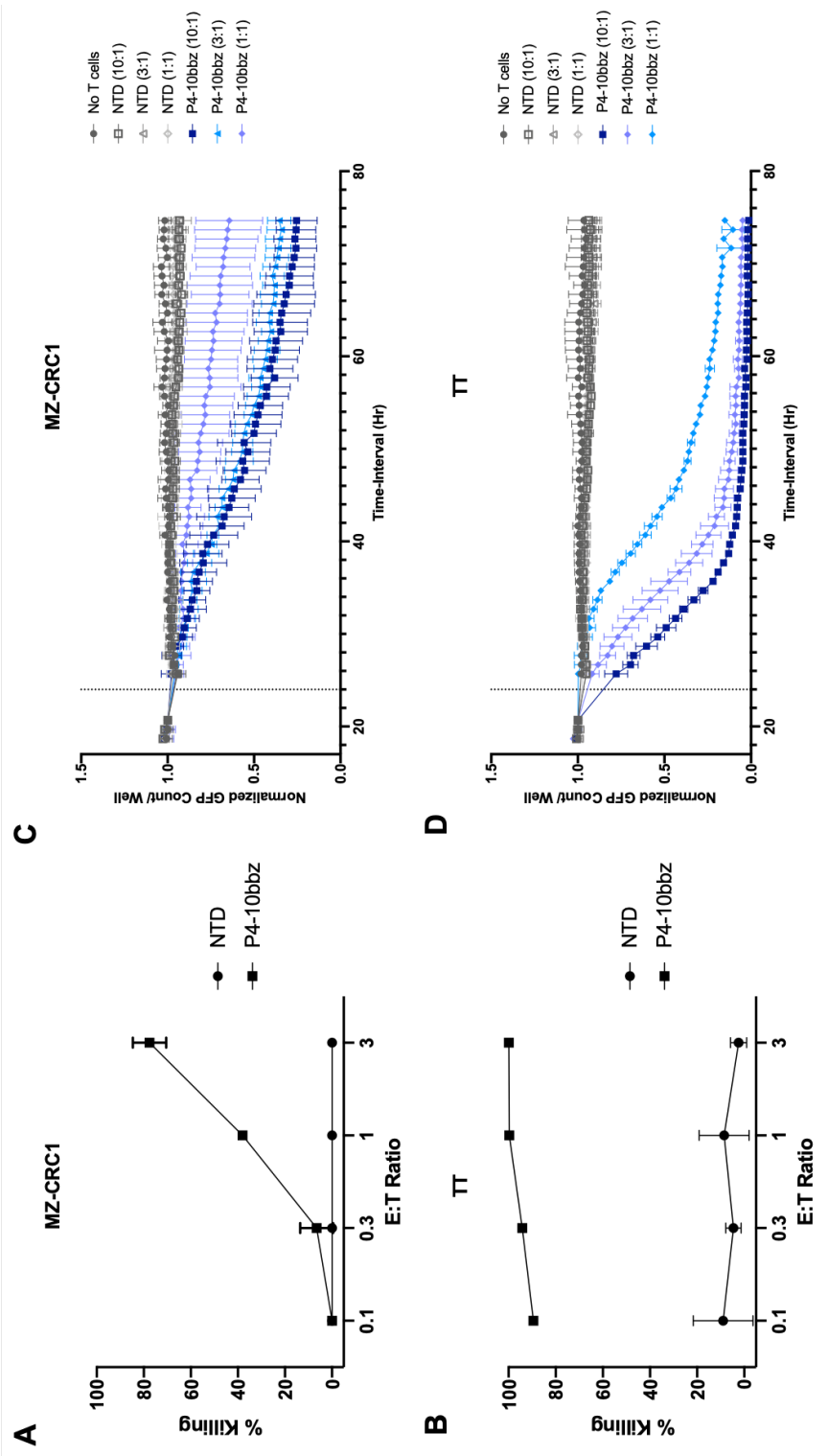

Figure S5. Lysis of MZ-CRC1 and TT cells by P4-10bbz CAR T cells. (A, B) Primary T cells expressing the P4-10bbz, or no CAR (NTD) were co-cultured with MZ-CRC1 or TT cells engineered to express click-beetle-green luciferase. After 96 hours of co-culture luciferin was

added to culture wells and the level of luminescence was measured to determine % lysis. Error bars represent one standard deviation. **(C, D)** MZ-CRC1 or TT cells engineered to express GFP were plated and GFP^+ cells were imaged over time using an xCelligence RTCA eSight instrument. 24 hours later (dotted line), primary T cells expressing the P4-10bbz, or no CAR (NTD) were added to the MZ-CRC1 and TT cells and GFP^+ cells were counted to determine lysis of target cells. Counts are normalized to values prior to addition of T cells. Error bars represent one standard deviation.

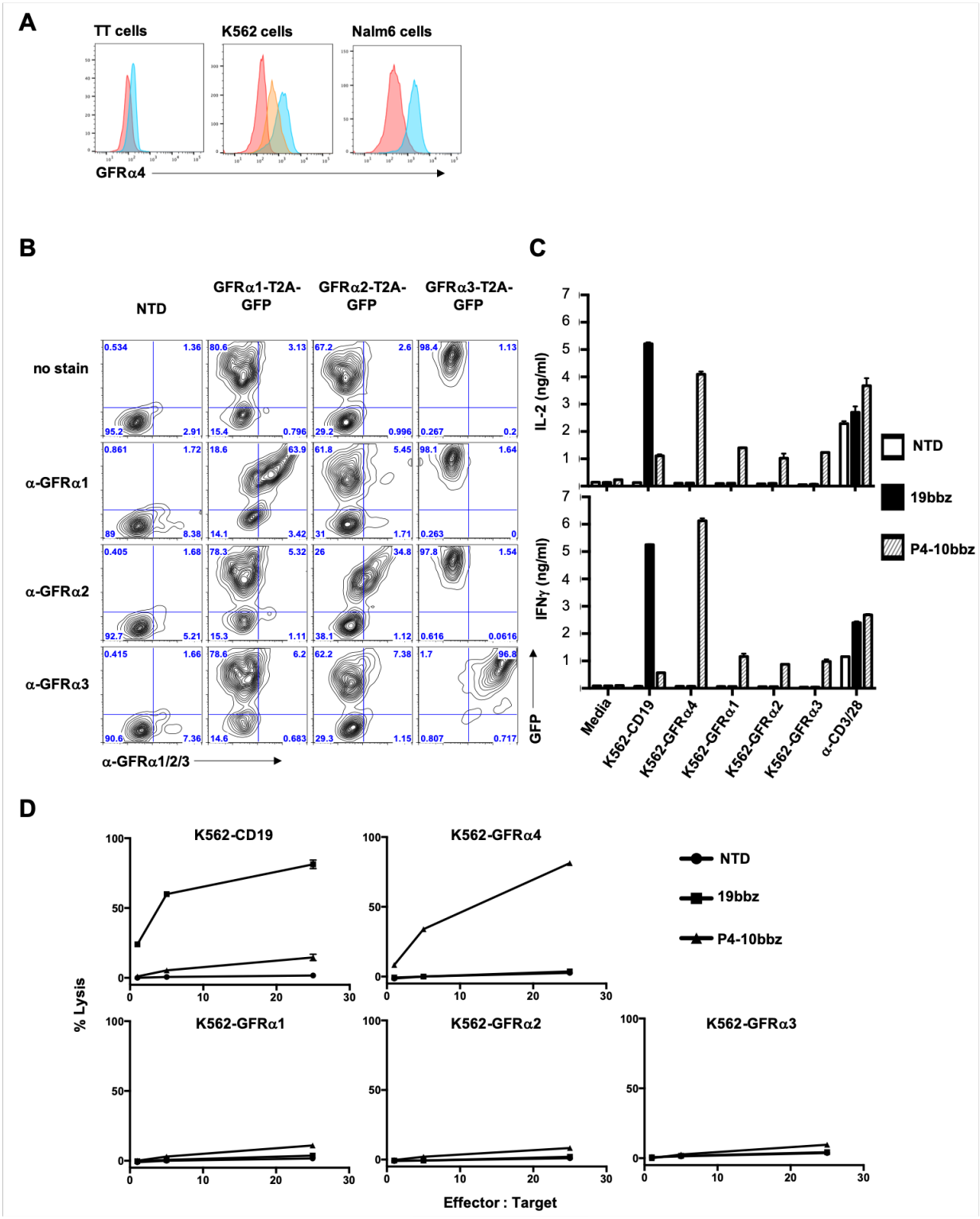

Figure S6. P4-10bbz targets K562 cells expressing GFRα4 but not GFRα1, GFRα2, or GFRα3. (A) TT cells were stained with P4-10 antibody (blue histogram, MFI=151) or was left unstained (MFI=89). P4-10 antibody staining was also performed on wild-type K562 cells (red

histogram, MFI=141), K562 engineered to express GFRα4a (orange histogram, MFI=515) or GFRα4b (blue histogram, MFI=1192) and on wild-type Nalm6 cells (red histogram, MFI=232) and Nalm6 engineered to express GFRα4b (blue histogram, MFI=1688), the latter used for experiments in Fig 4d. **(B)** GFRα1, 2, and 3 expression was measured on K562 cells engineered to express the indicated human GFR family member, each linked to GFP. **(C)** Culture supernatant IL-2 and IFNγ was measured following overnight co-culture of primary human T cells expressing not CAR (NTD), or the indicated CARs, with target K562 cells as in (A) or with anti-CD3/anti-CD28 coated beads. **(D)** Primary human T cells expressing no CAR (NTD) or the indicated CARs were co-cultured for approximately 18 hours with Cr51-loaded TT cells or K562 cells expressing the indicated antigens, at the indicated effector : target ratios. Following co-culture, supernatant was assessed for released radioactivity. % Lysis was calculated according to the formula: 100*((experimental – spontaneous)/(maximum – spontaneous), where spontaneous represents radioactivity released from cultures of target cells alone and maximum represents radioactivity release by target cells lysed with 5% SDS. Error bars represent 1 standard deviation of three technical replicates. Results in (A), (C), and (D) are representative of at least 2 independent experiments.

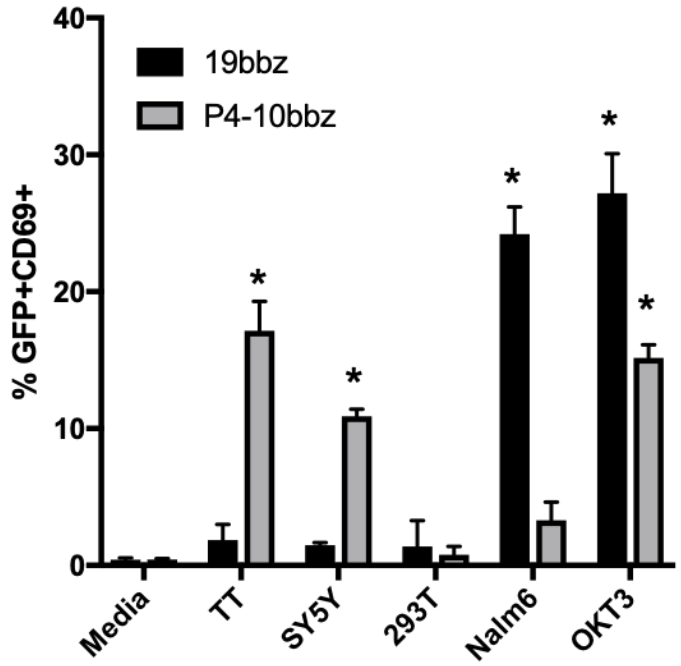

Figure S7. P4-10bbz is activated by MTC (TT) and a neuroblastoma cell line (SY5Y). NFAT-GFP reporter Jurkat cells expressing 19bbz or P4-10bbz were co-cultured overnight with the indicated stimuli, followed by assessment of $GFP^{+}CD69^{+}$ expression in the Jurkat cells by flow cytometry (* $p<0.05$, ANOVA with Dunnett's multiple comparisons test compared to media control for each CAR).

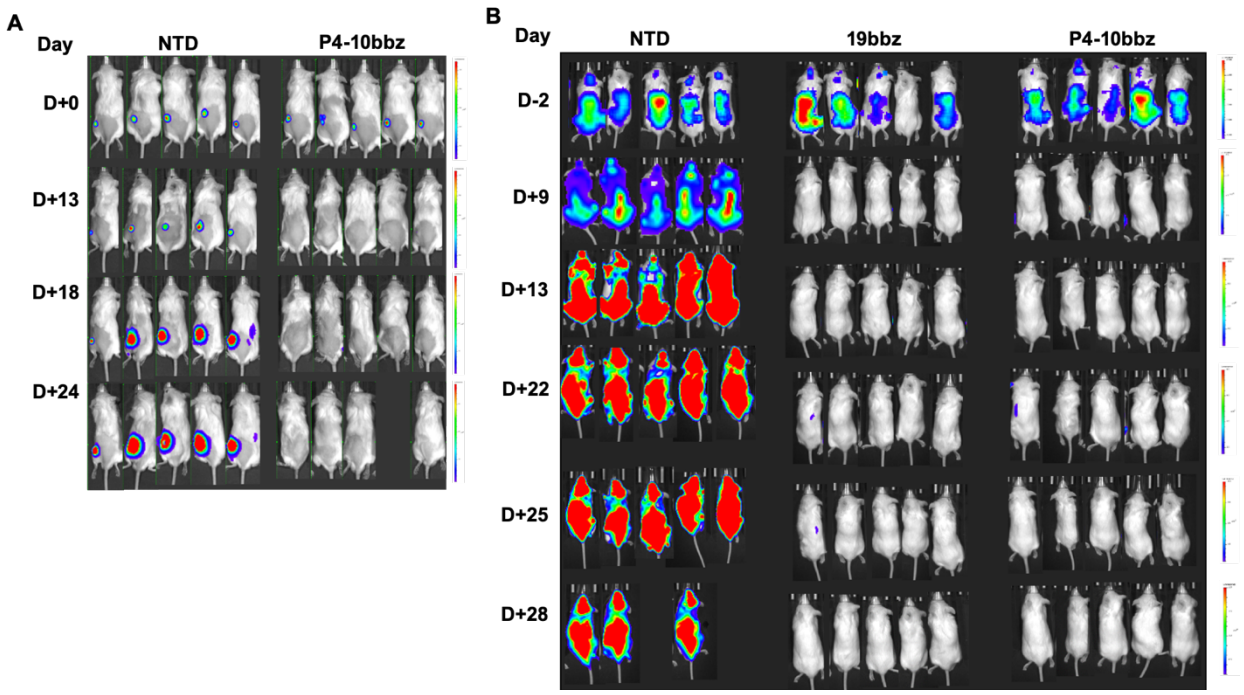

Figure S8. Bioluminescence images of mice from experiments shown in Figure 4a and 4d. Following TT cell engraftment **(A)** and Nalm6 **(B)** engraftment**,** T cells were injected on Day 0 and mice were imaged on indicated days.

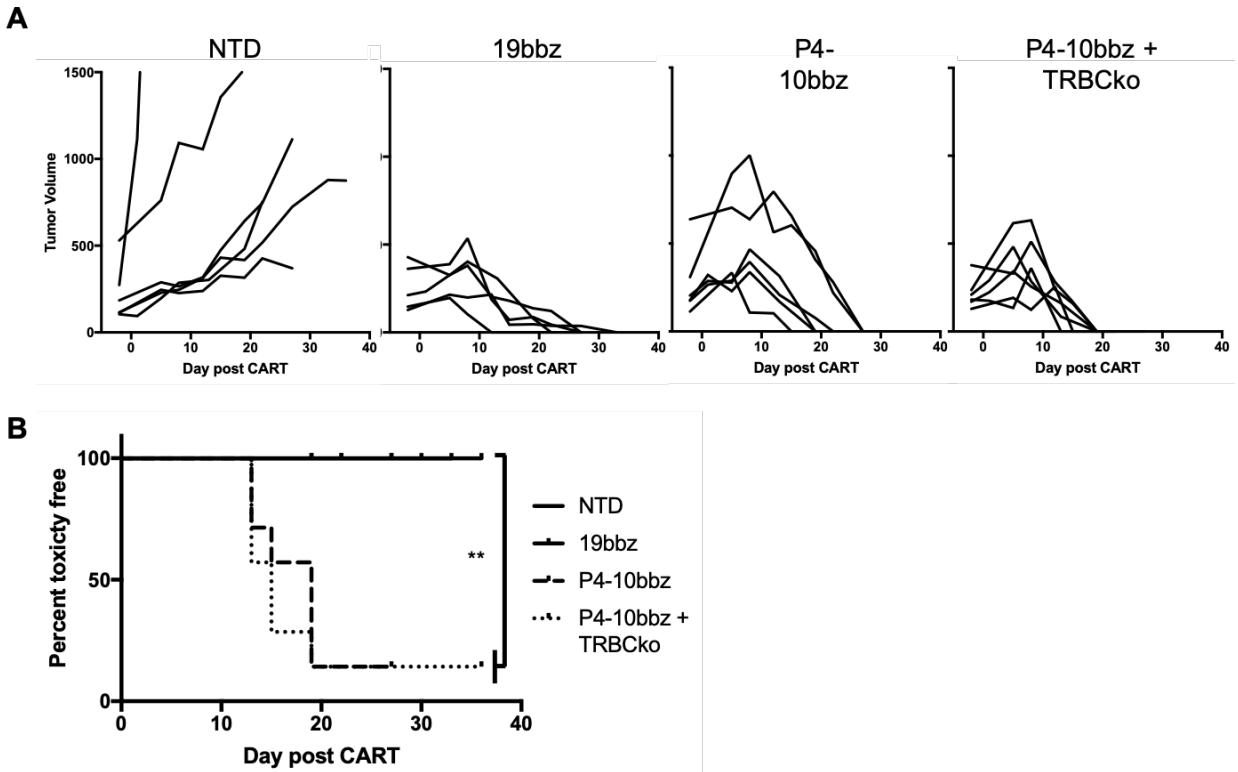

Figure S9. Skin toxicity is mediated by P4-10bbz CAR. NSG mice were injected with $5x10^6$ TT cells engineered to express CD19. When tumors reached approximately $100mm^3$, mice were injected intravenously with $1x10^7$ T cells expressing no CAR (NTD, n=6), 19bbz (n=5), P4-10bbz (n=6), or T cells expressing P4-10bbz in which the TRBC was disrupted by CRISPR-Cas9 (n=6). Tumor volumes were measured by caliper measurement (A) and incidence of skin toxicity was assessed by gross observation (B). Curves in (A) represent individual mice. * $p<0.005$ Log-rank test.

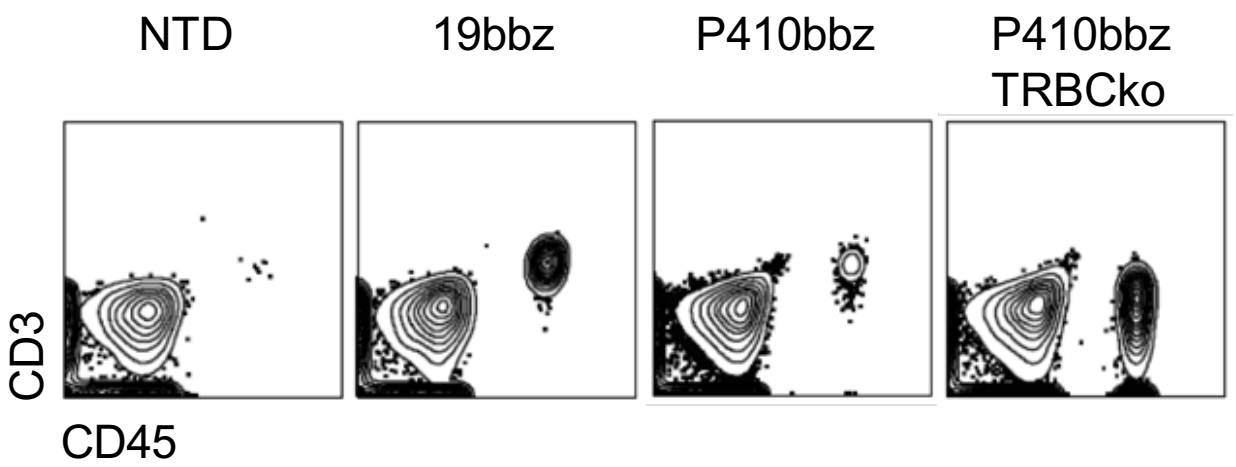

Figure S10. T cells in the blood of the TRBC-ko group remain surface CD3-neg. NSG mice, as shown in Figure S5, were injected with $5x10^6$ TT cells engineered to express CD19. When tumors reached approximately $100mm^3$, mice were injected intravenously with $1x10^7$ T cells expressing no CAR (NTD, n=6), 19bbz (n=5), P4-10bbz (n=6), or T cells expressing P4-10bbz in which the TRBC was disrupted by CRISPR-Cas9 (n=6). On Day 20 post T-cell injection, mice were bled, and samples were stained with antibodies against CD8, CD3, CD4, and CD45 followed by flow cytometric analysis. Representative plots from each group are shown.

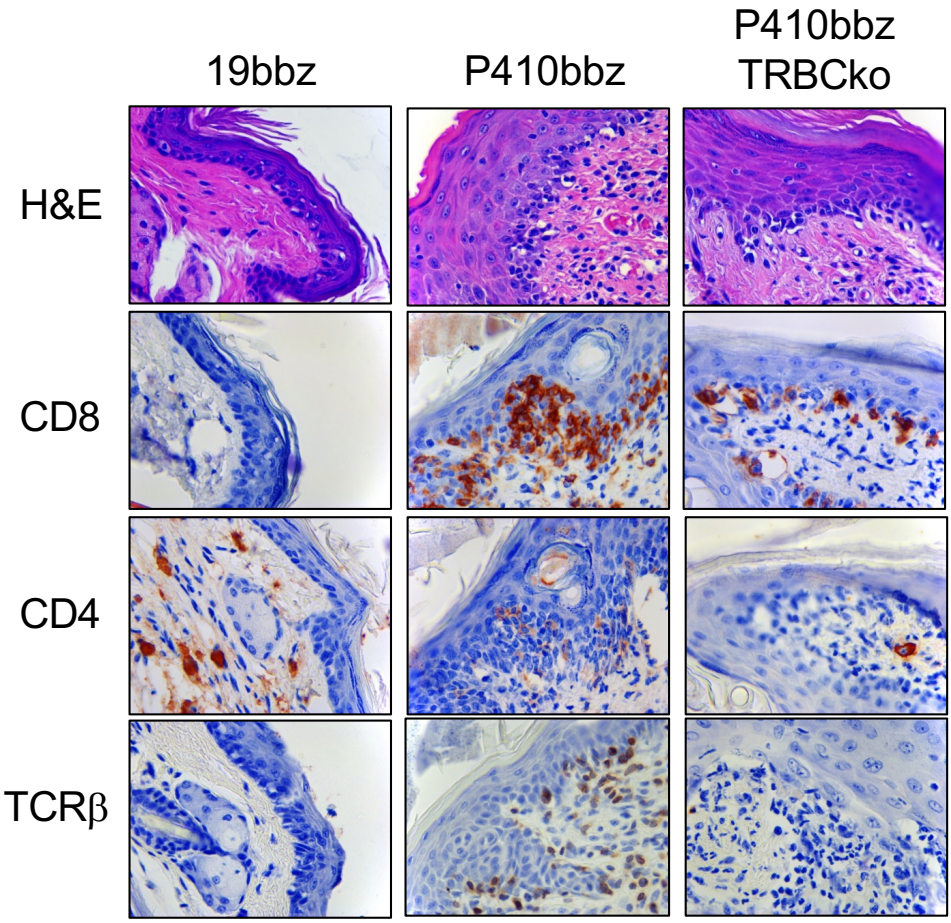

Figure S11. T cells in the skin of the TRBC-ko group remain TCR-β negative. NSG mice, as shown in Supplemental Figure 5, were injected with $5x10^6$ TT cells engineered to express CD19. When tumors reached approximately $100mm^3$, mice were injected intravenously with $1x10^7$ T cells expressing no CAR (NTD, n=6), 19bbz (n=5), P4-10bbz (n=6), or T cells expressing P4-10bbz in which the TRBC was disrupted by CRISPR-Cas9 (n=6). After mice were euthanized, skin was analyzed by hematoxylin and eosin staining and by immunohistochemistry with antibodies specific for human CD8, CD4, and TCR-β. Representative sections from the indicated groups are shown.

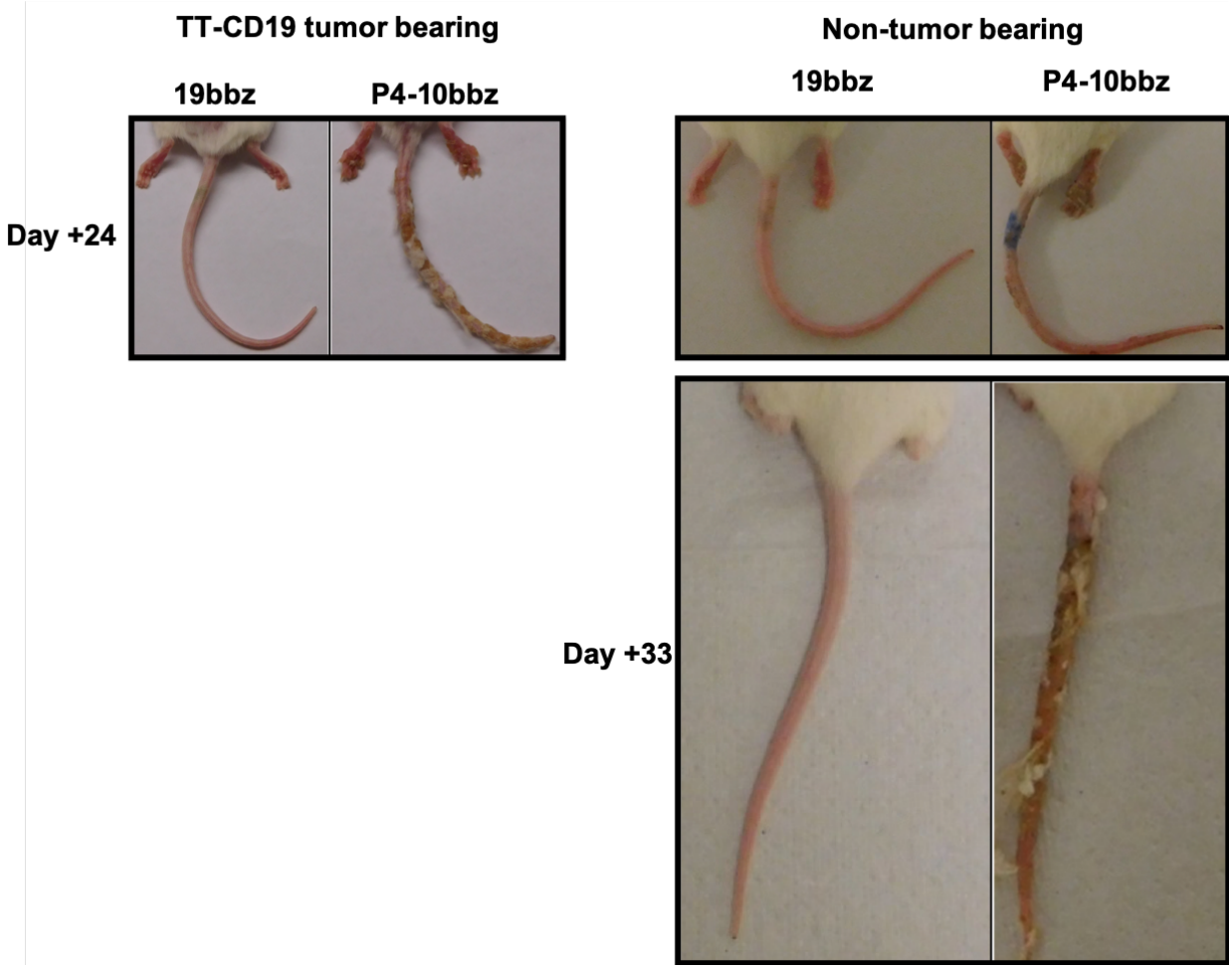

Figure S12. Skin toxicity resulting from P4-10bbz CAR is independent of tumor. NSG mice with and without subcutaneously implanted TT-CD19 tumor cells received T cells expressing 19bbz or P4-10bbz. By day 24, tumors were cleared in both 19bbz and P4-10bbz treated tumor bearing mice and P4-10bbz treated mice developed skin toxicity. In non-tumor bearing mice, P4-10bbz treated mice also developed skin toxicity but with slower kinetics.

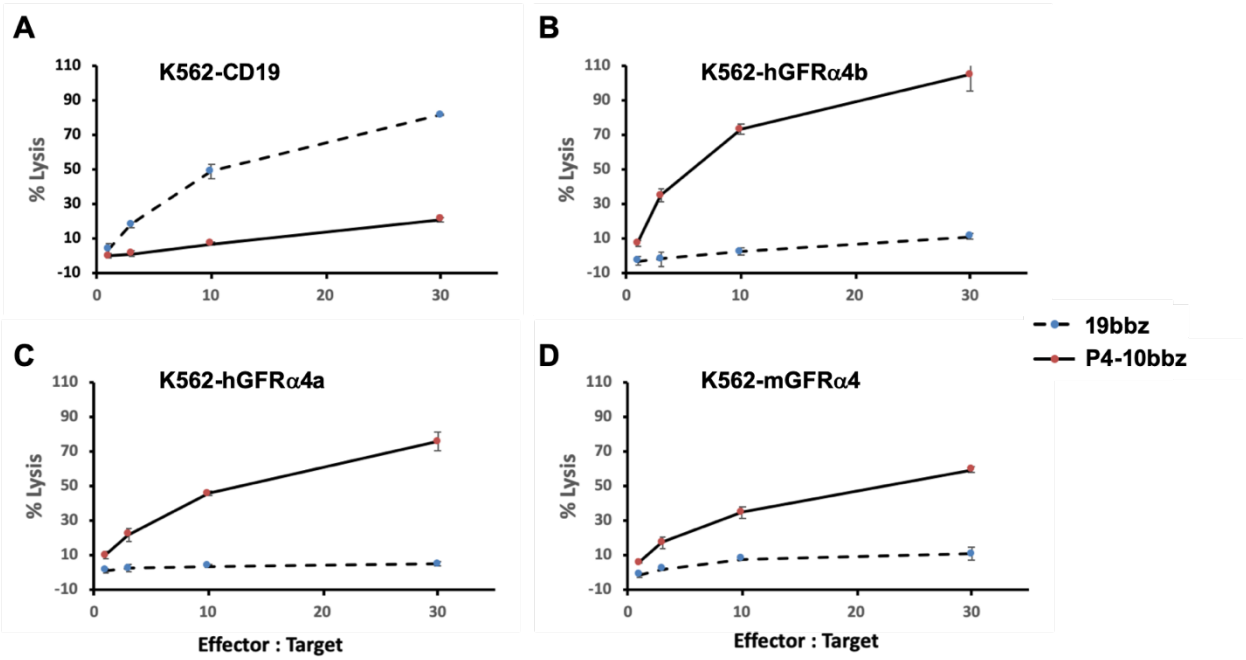

Figure S13. P4-10bbz CAR targets murine GFRα4 expressed on K562 cells. Primary T cells expressing the 19bbz or P4-10bbz CAR were co-cultured with ^{51}Cr-loaded K562 cells engineered to express human CD19 (A), human GFRα4b (B), human GFRα4a (C), or murine GFRα4 (D). After overnight co-culture at the indicated effector:target ratios, supernatants were harvested and released radioactivity was measured to determine % lysis. Error bars represent one standard deviation of technical triplicates.

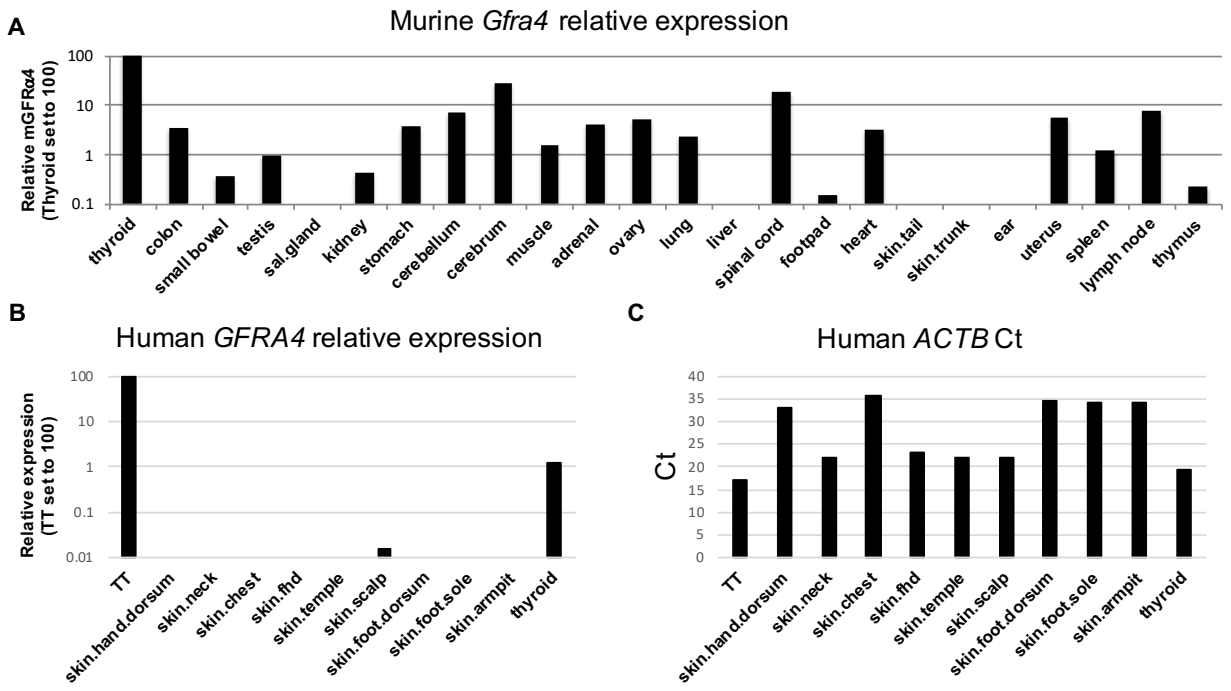

Figure S14. Murine *Gfra4* and human *GFRA4* mRNA are not detected in skin by qPCR. (A) Relative *Gfra4* transcript level measured by qPCR of cDNA created from various murine tissue samples. The signal from tissues is relative to thyroid which was set to 100. Transcript levels are normalized to β-actin as a housekeeping gene. (B) Relative *GFRA4* transcript level measured by qPCR of cDNA created from various human skin samples, human thyroid and TT cells. The signal from tissues is relative to TT cells which was set to 100. Transcript levels are normalized to β-actin as a housekeeping gene. (C) The Ct level of amplification of β-actin (ACTB) transcripts from samples shown in (B).

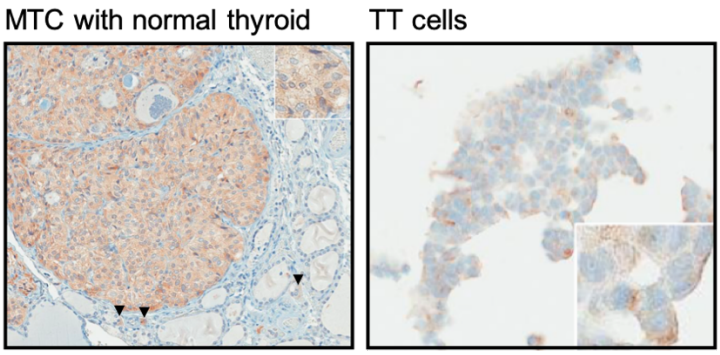

Figure S15. Immunohistochemistry using P4-10 antibody. A sample of MTC with adjacent normal thyroid (left) and TT cells (right) were stained with P4-10 antibody. Positively staining parafollicular cells are indicated with arrowheads.

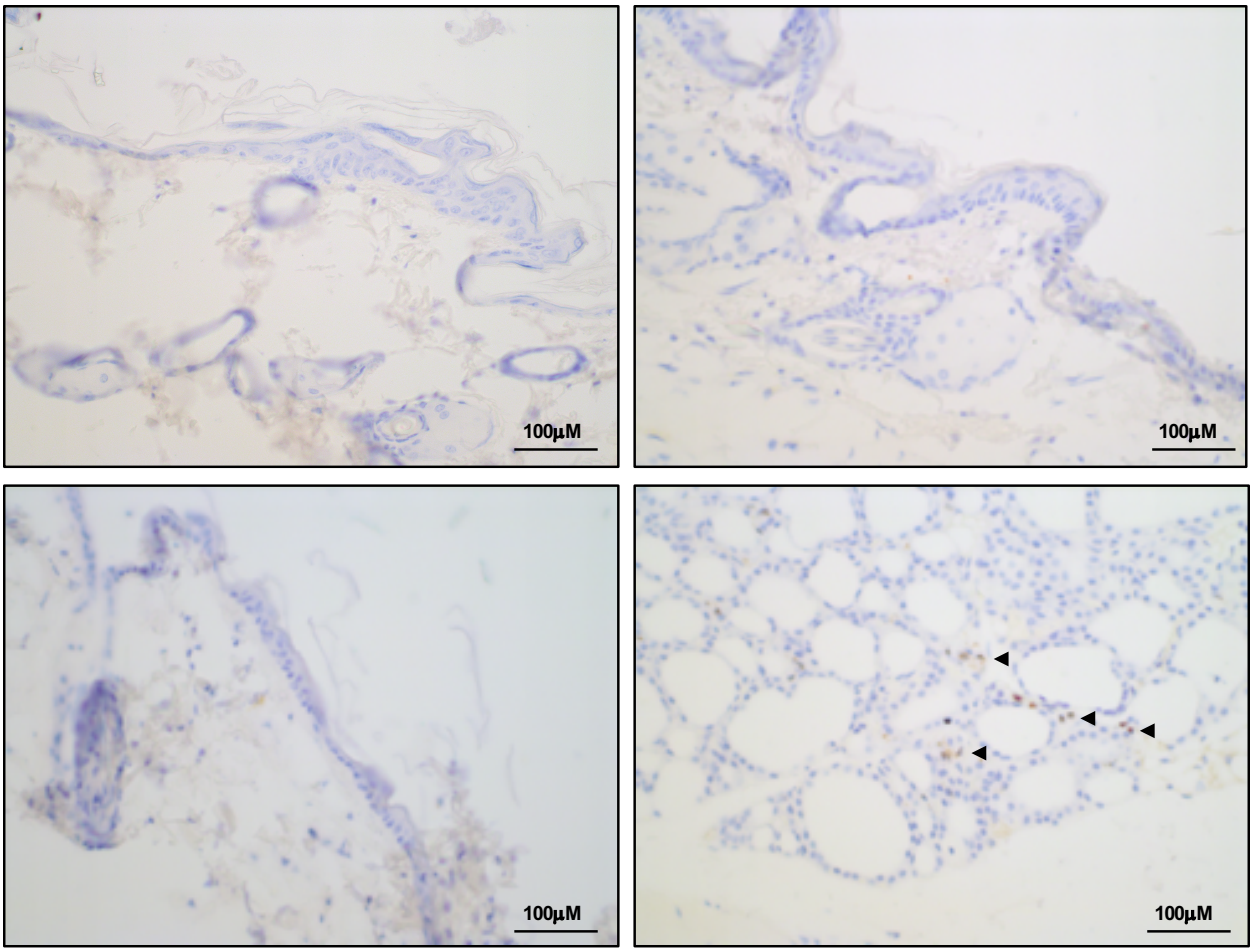

Figure S16. *Gfra4* mRNA is detected in murine thyroid but not skin. Murine ear, tail, and flank skin and murine thyroid (bottom right) were tested by RNA in situ hybridization (RNAscope) using probes specific for murine *Gfra4* mRNA. Arrowheads indicate areas with positively staining cells.

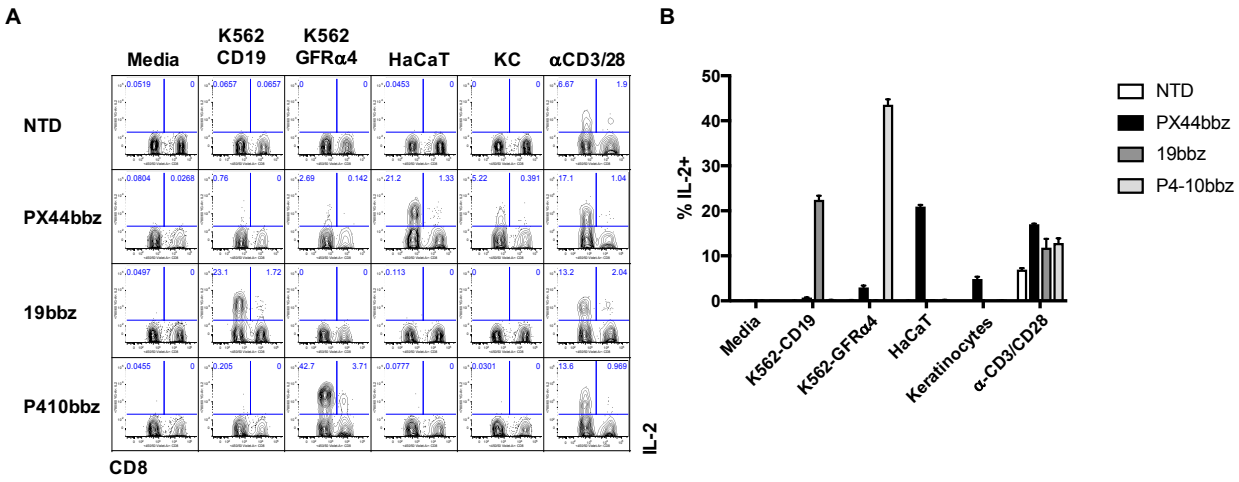

Figure S17. Primary P4-10 CAR T cells do not react to human keratinocytes. (A) Primary human T cells expressing no CAR (NTD), PX44bbz, 19bbz, or P4-10bbz were co-cultured for 6 h with the indicated target cells or with anti-CD3/anti-CD28 coated beads. Following co-culture, cells were fixed, permeabilized and stained for intracellular IL-2 and surface CD8 and analyzed by flow cytometry. Representative plots of replicates are shown. KC = primary human keratinocytes. **(B)** Percentage of IL-2^{+} T cells from (A) is shown for each condition. Error bars represent one standard deviation of technical replicates.

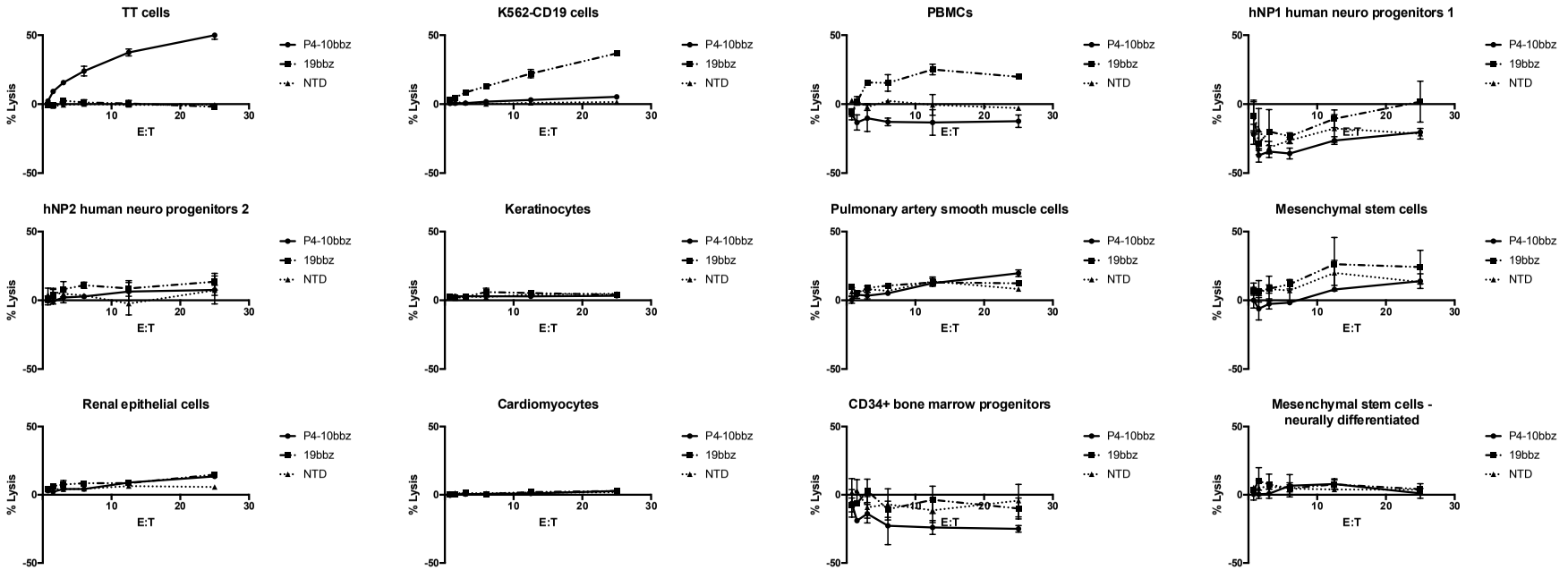

Figure S18. P4-10bbz CAR T cells specifically target TT cells but not a panel of human primary cells. Primary T cells expressing the 19bbz, P4-10bbz, or no CAR (NTD) were co-cultured with ^{51}Cr-loaded primary human cells, TT cells, and K562-CD19 cells at the indicated effector:target ratios. After 4 h of co-culture supernatants were harvested and released radioactivity was measured to determine % lysis. Error bars represent one standard deviation.

Heavy chains	V region germline gene	% Human homology	FR1	CDR1	FR2	CDR2	FR3	CDR3	FR4
P410	Rabbit IGHV1S34*01	54%	QSVKESEGGLFKPTDTLTLTCTVSGFSLS	RHALT	WVRQAPGNGLEWIG	AIDNAGTTYYASWAKS	RSTITRNTDLHTVTLKMTSLTASDTATYFCAR	VFYDINSGYYLDGMDL	WGPGTLVTVSS
CAR25	Human IGHV4-38-2*02	85%	QVQLQESGPGLVKPSETLSLTCAVSGYSIS	RHALT	WIRQPPGKGLEWIG	AIDNAGTTYYASWAKS	RVTISVDTSKNQFSLKLSSVTAADTAVYYCAR	VFYDINSGYYLDGMDL	WGPGTLVTVSS
CAR29	Human IGHV3-48*03	85%	EVQLVESGGGLVQPGGSLRLSCAASGFTFS	RHALT	WVRQAPGKGLEWVS	AIDNAGTTYYASWAKS	RFTISRDNAKNSLYLQMNSLRAEDTAVYYCAR	VFYDINSGYYLDGMDL	WGPGTLVTVSS
Light chains									
			FR1	**CDR1**	**FR2**	**CDR2**	**FR3**	**CDR3**	**FR4**
P410	Rabbit IGLV4S4*01	70%	QFVLTQSPSVSAALGASAKLTC	TLSSAHKTYTID	WYQQQQGEAPRYLMQ	VKSDGSYTKGT	GVPDRFSGSSSGADRYLIIPSVQADDEAGYVC	GADDNGGYV	FGGGTQLTVT
CAR25/CAR29	Human IGLV4-69*01	85%	QLVLTQSPSASASLGASVKLTC	TLSSAHKTYTID	WYQQQPEKGPRYLMQ	VKSDGSYTKGT	GVPDRFSGSSSGADRYLTISSLQSEDEADYYC	GADDNGGYV	FGGGTQLTVL

Figure S19: Sequence analysis of rabbit and humanized P4-10 variable regions. Heavy and light chain variable region gene assignments were determined using IMGT Domain-GapAlign tool (37).

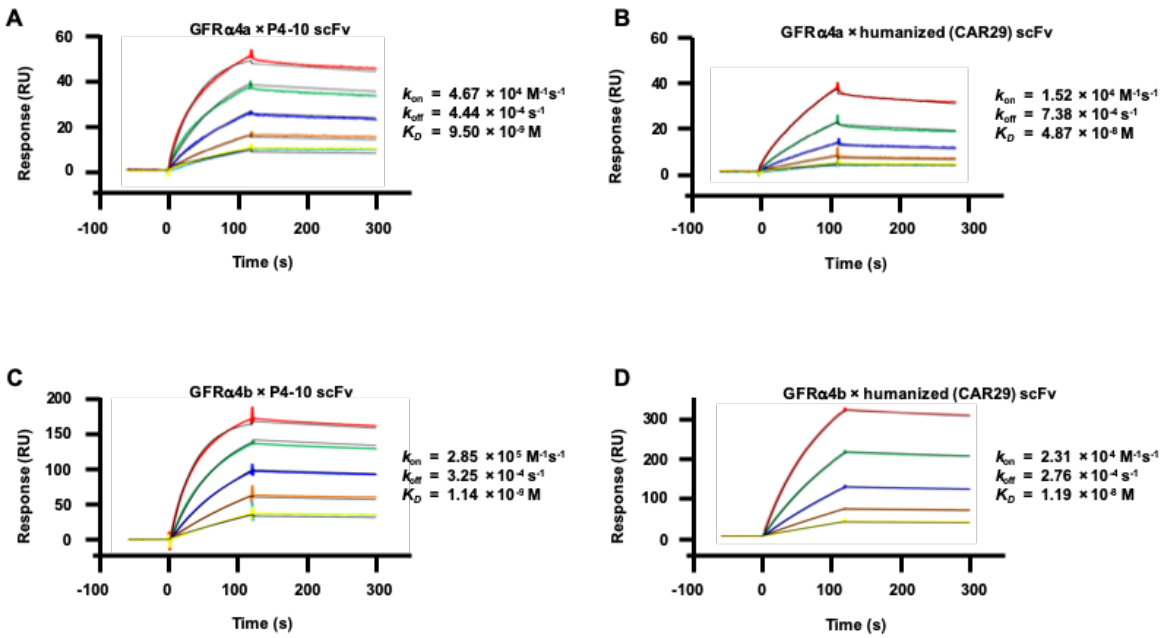

Figure S20. SPR analysis of the binding of scFv to GFRα4. huFc-GFRα4a (**A, B**) or huFc-GFRα4b (**C** and **D**) were captured via a mouse anti-human IgG C_{H2} monoclonal antibody immobilized on a sensor chip, followed by injection of rabbit scFv (**A** and **C**) or humanized scFv (**B** and **D**) at five concentrations, serially diluted by two-fold from the highest concentration (100 nM for **C** and 500 nM for **A**, **B**, and **D**) with a replicate of the lowest concentration to confirm regeneration of the sensor chip. Sensorgrams show the response (RU, resonance units) plotted against time (s, seconds). Colored lines are the experimental tracings obtained from the SPR experiments and black lines are the best global fits (1:1 Langmuir binding model) used to calculate the association (k_{on}) and dissociation (k_{off}) rate constants. The equilibrium dissociation constant (K_D) was calculated as k_{off}/k_{on}.

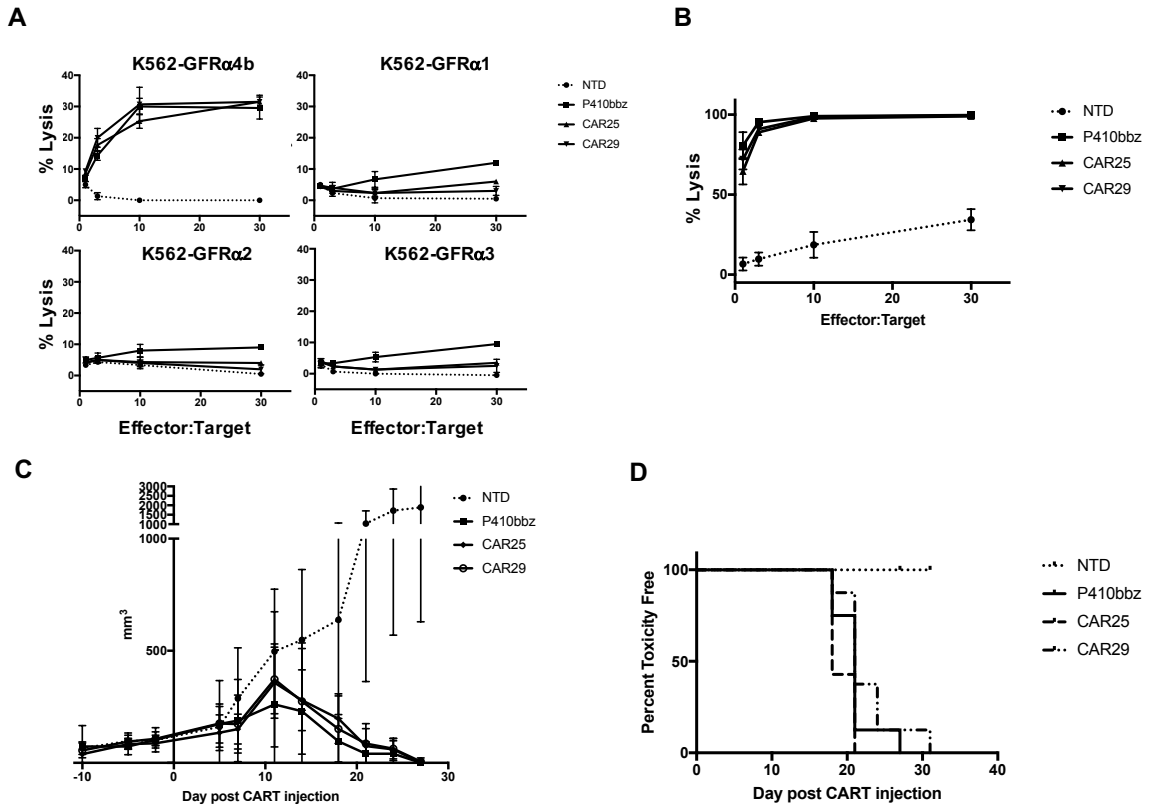

Figure S21. Humanized P4-10bbz CARs demonstrate equivalent efficacy *in vitro* and *in vivo*. (A, B) Human T cells expressing the indicated CARs or no CAR (NTD) were co-cultured overnight with ^{51}Cr-loaded K562 cells expressing GFRα1, GFRα2, GFRα3, or GFRα4b (A) or with ^{51}Cr-loaded TT cells (B) at the indicated effector to target ratios. Culture supernatants were harvested and assayed for radioactivity and % lysis was calculated according to the formula: 100*((experimental-spontaneous)/(maximum/spontaneous)). Error bars represent one standard deviation. (C) TT tumor volumes measured over time in NSG mice treated with 5 x 10^6 P4-10bbz (n=8 mice), CAR25 (n=7 mice), or CAR29 (n=8 mice) CAR T cells or an equivalent number of non-transduced cells (NTD, n=7 mice) 10 days after subcutaneous implantation of 5 x 10^6 wild-

type TT cells. Curves plot means of tumor volumes +/- one standard deviation for each experimental group.